TURBOMACHINERY & PUMP SYMPOSIA | HOUSTON, TX
SEPTEMBER 26-28, 2023
SHORT COURSES: SEPTEMBER 25, 2023

AXIAL VIBRATIONS DUE TO ACOUSTIC AND ROTORDYNAMIC RESONANCES IN A DRY SCREW COMPRESSOR

Dominic Maton
Senior Machinery Engineer
ExxonMobil
Singapore

Ben Davies
Principal Rotating Equipment Engineer
SBM Offshore
Monaco

Luis A. Rojas
Machinery Senior Principal
ExxonMobil
Houston, Texas, USA

Cyril Mouries
Asset Integrity Production Strategy Manager
SBM Offshore
Monaco

Tobias Wiedemann
Head of Mechanics & Rotor Dynamics
MAN Energy Solutions
Oberhausen, Germany

Philipp Köster
Project Engineer, Mechanics & Rotor Dynamics
MAN Energy Solutions
Oberhausen, Germany

Stephen Price
President
Engineering Dynamics, Inc.
San Antonio, Texas, USA

C. Hunter Cloud
President
BRG Machinery Consulting, LLC
North Garden, Virginia, USA

Dominic A. Maton is Senior Machinery Engineer with ExxonMobil. Mr. Maton is responsible for providing Machinery Expert Support for ExxonMobil Projects and Operations globally. Mr. Maton earned his BSME (1989) from Curtin University of Technology (Western Australia). He began his career with Exxon in 1990 as a Mechanical Engineer and has focused on turbomachinery for most of his career. Mr. Maton has had multiple assignments globally with both Operations and Project. Mr. Maton is currently based in Singapore.

Ben Davies is a Principal Rotating Equipment Engineer with SBM Offshore, located in Monaco. Mr. Davies earned his M.Eng (2009) from University of Bristol (UK) and has 14 years of experience with offshore oil and gas projects and machinery. Mr Davies is responsible for providing machinery support within SBM Offshore for new projects and the operating FPSO fleet.

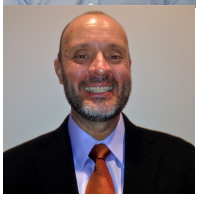

Luis Rojas is the ExxonMobil Machinery Senior Principal. Mr. Rojas provides technical leadership to global operations and projects. He received his BSME (1986) and MSME (1989) from The Ohio State University. Started his career as Rotating Equipment Engineer in Lagoven in Maracaibo, Venezuela. Joined Dresser-Rand in 1995 as Technical Support Engineer in Olean NY, and became Director of Availability Plus in 2000 in Houston TX. Mr. Rojas joined ExxonMobil in 2002 as a Machinery Engineer in US Production, and has had multiple international assignments including Nigeria, Qatar and Papua New Guinea, providing support to onshore, offshore and LNG operations and projects.

Cyril Mouries is Asset Integrity Production Strategy Manager with SBM Offshore, located in Monaco. Mr. Mouries earned is mechanical engineer degree (1996) from École centrale Méditerranée and has 22 years of experience in the oil & gas industry as a turbomachines specialist. Before joining SBM Offshore in 2018, he was successively responsible for application engineering for an OEM, lead machinery engineer for EPC companies, and later consultant for major O&G clients. During his career, he participated in multiple projects, both on and offshore, where he contributed to engineering, installation, commissioning, start-up, operation and maintenance of major rotating equipment. In addition to providing machinery support within SBM, he is in charge to define the Asset Integrity Operational strategies to ensure best in class production performance of SBM fleet.

Tobias Wiedemann is head of the department for mechanics & rotor dynamics for large trains of MAN Energy Solutions site in Oberhausen. In his role, his responsibilities include the analysis and further development of the mechanical components of large turbomachines, such as axial compressors, centrifugal compressors, steam turbines and expanders, as well as their complete trains. He is responsible for providing technical support in the areas of rotor dynamics and structural mechanics for assigned projects, the technical bid support and RCA. He received his Diploma in Mechanical Engineering (2003) and his Ph.D. (2009) from the Ruhr-University of Bochum. He joined MAN-ES in 2008 as calculation engineer for the mechanical assessment of axial and centrifugal compressors

Philipp Köster is working as a mechanical engineer in the department of mechanics & rotor dynamics for large trains at MAN Energy Solutions in Oberhausen. In his role as an expert in the field of structural mechanics, he is working on research and development projects for axial and centrifugal compressors and provides technical support for assigned projects and RCA. He received his Diploma in Mechanical Engineering (2006) and his Ph.D. (2014) from the University of Siegen. He joined MAN-ES in 2011 as calculation engineer for the mechanical assessment of axial and centrifugal compressors.

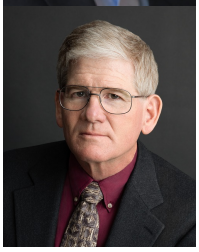

Stephen M. Price is President of Engineering Dynamics Inc. in San Antonio, TX. Mr. Price is responsible for performing analytical and field services in the areas of vibration, pulsation, stress analysis, fluid flow, and acoustics. Mr. Price earned his BSME (1983) from Mississippi State University and his MSME (1985) at Purdue University. He is a Registered Professional Engineer in the state of Texas and a member of the the advisory committee for the Texas A&M Turbomachinery Symposium. Mr. Price has authored several technical papers in the areas of reciprocating and rotating machinery and measurement and signal processing techniques. He has also been the major contributor in the design and development of complex data acquisition and long-term monitoring systems.

C. Hunter Cloud is President of BRG Machinery Consulting, LLC, located near Charlottesville, Virginia, a company providing a broad range of rotating machinery technical services. He began his career with Mobil Research and Development Corporation in Princeton, NJ, as a turbomachinery specialist responsible for application engineering, commissioning, and troubleshooting for production, refining and chemical facilities. During his 11 years at Mobil, he worked on numerous projects, including several offshore gas injection platforms in Nigeria as well as serving as reliability manager at a large US refinery. Dr. Cloud received his BSME (1991) and Ph.D. (2007) from the University of Virginia. He is a member of ASME, the Vibration Institute, the API 617 and API 684 task forces, and the advisory committee for the Texas A&M Turbomachinery Symposium.

ABSTRACT

During commissioning of a large FPSO, a dry screw compressor in a flash gas service experienced significant failures related to high axial vibration at 2× rotor speed. There were also excessive pulsation and vibration levels measured at the compressor, discharge silencer and downstream piping at 4× rotor speed ("pocket pass frequency" or PPF). Eventually, fatigue failures occurred within the compressor and in the downstream systems.

This paper describes the collaborative effort amongst the designer/operator, user company, equipment OEM and consultants to determine the root cause(s) as well as design and implement solutions. The remarkable discovery was that the axial rotordynamics and the 3-dimensional acoustics were actually interrelated. Non-linear, time transient axial dynamics simulations were needed as well as advanced 3D acoustic analyses of the compressor discharge system that are well beyond

typical analyses performed for API 619 machines. These analyses, along with extensive field measurements, led to the eventual solution. Comprehensive factory testing was a key factor in proving the solution before implementing the fix offshore. Both rotordynamics and acoustical modifications were required to ensure successful, long-term operation of the dry screw compressor.

INTRODUCTION

An API 619 dry screw compressor installed on a floating, production, storage, and offloading (FPSO) facility in South America experienced significant operational challenges leading to compressor failures. The aim of this paper is to detail the challenges experienced by the screw compressor, and the detailed rotordynamic and acoustical modelling, development testing and subsequent design modifications that led to the resolution of the operational problems.

The FPSO has two flash gas compressor (FGC) packages operating in series consisting of three compressor stages. The failures were limited to the third stage compressor. The initial compressor failure occurred very shortly after start-up and was identified after a machine trip due to high compressor casing vibration. The failure was significant with rotor and casing contact, significant amount of fretting damage, and a large shaft crack. The compressor experienced multiple repeat failures over the following two years, including thrust bearing damage, rotor contact, rotor lock nuts loosening, and seal failures.

The same compressor also experienced multiple compressor discharge silencer failures which, although not covered in this paper, factor into some of the modifications and testing on the compressor. Some of the modifications made to the acoustic suppression system design did have a detrimental impact on the compressor vibration, but also provided important observations which eventually led to a final successful solution.

The investigation carried out for the various failures discovered that interactions between complex rotordynamic and acoustic phenomena were leading to high axial vibration, eventually leading to compressor failures. Modifications further detailed in this paper to the acoustical and rotordynamic design of the screw compressor design were developed to rectify the operational problems.

Machine and Process Description

Shown in Figure 1, the FPSO's Flash gas system has three stages of compression configured in two compressor packages FCC-LP (1st Stage) and FGC-MP (2nd and 3rd Stages). The compressors are screws with mechanical oil seals. These gas compressors process gas from the crude oil system where it is later reinjected as illustrated in Figure 2. The third stage screw compressor is driven, together with the second stage screw compressor, by a fixed speed electric motor, and a double stage speed increasing gearbox all located on a single baseplate (FGC - MP Compressor).

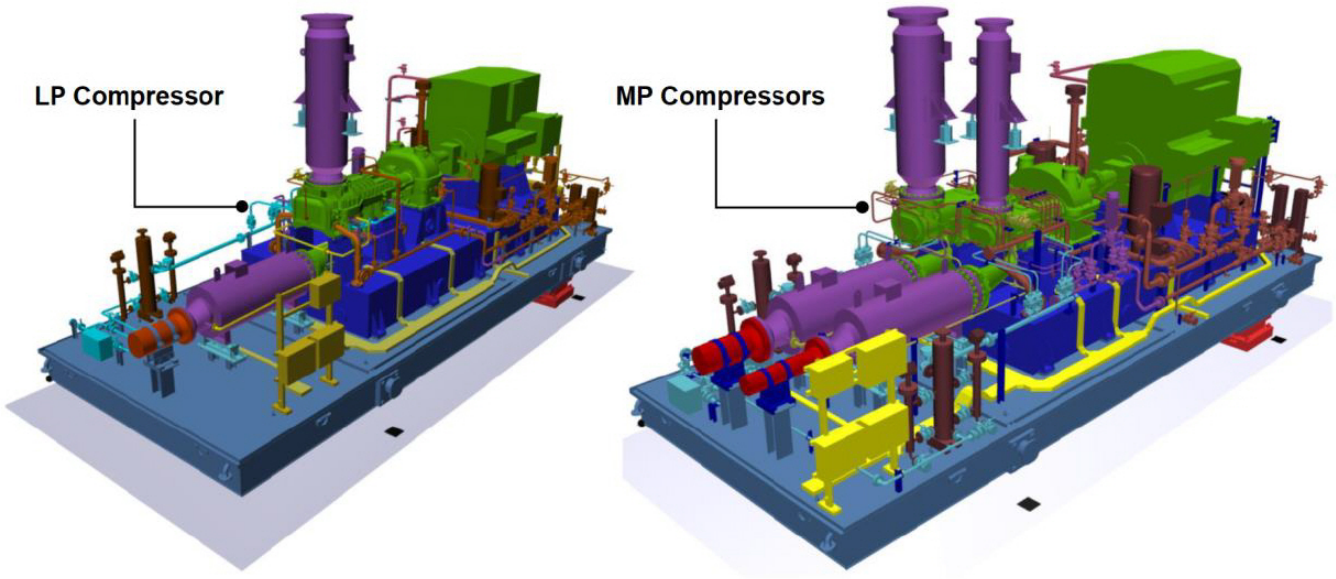

Figure 1: LP and MP compressor packages

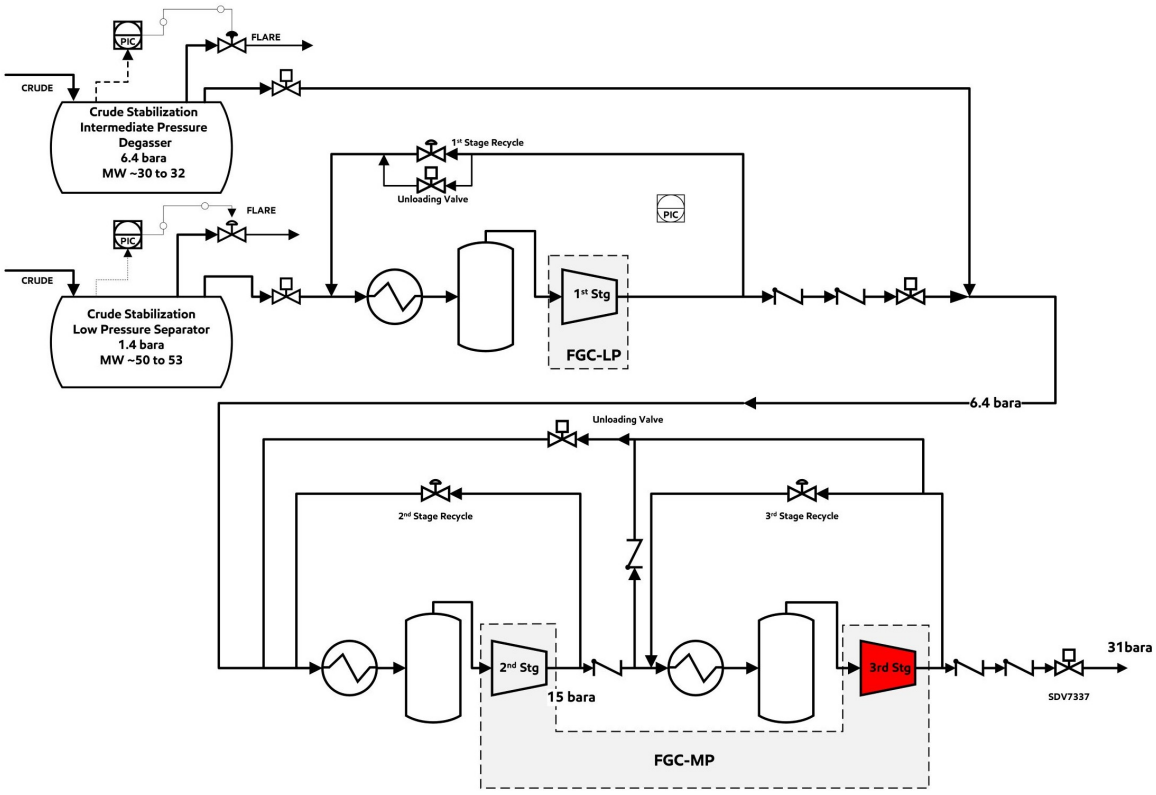

Figure 2: Flash gas system process flow diagram

For each compressor, the male rotor (MR) is connected to the gearbox pinion with a torsion shaft. The MR is connected to the female rotor (FR) through timing gears. Each MR has a thrust bearing on the drive end and uses the torsion shaft connecting hub as the active side's thrust collar as illustrated in Figure 3.

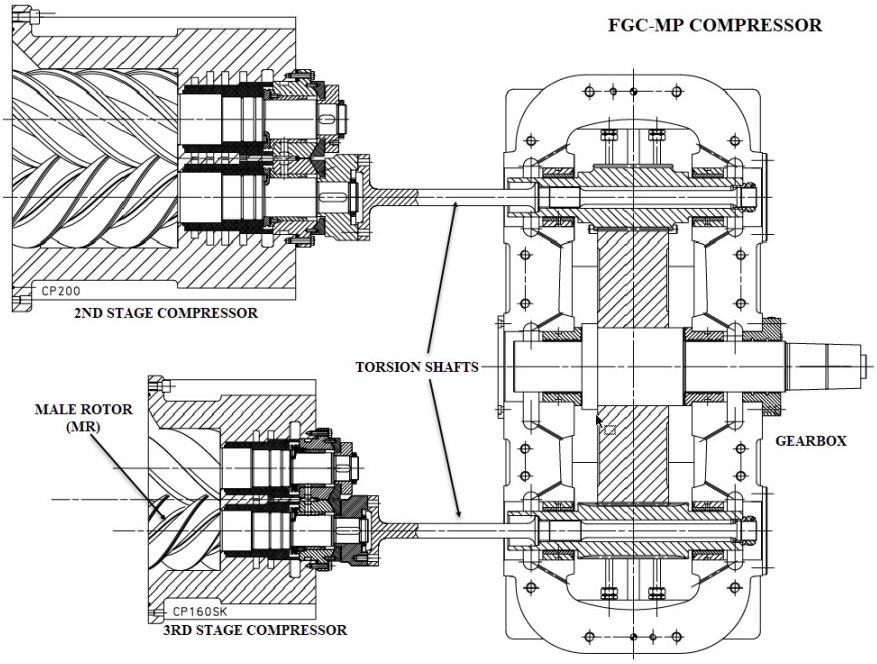

Figure 3: MP compressor configuration

Engineering Dynamics Incorporated
16117 University Oak, San Antonio, TX 78249
210-492-9100 www.engdyn.com

The design of the oil free screw compressor drive train is shown in Figure 4. Both male and female rotors run in cylindrical, radial journal bearings. The pressure on the screw profile causes a defined axial thrust towards the suction side of approximately 13 kN, which acts on the active side of the bearing. The total end float clearance of the MR is 90 μm, which is adjusted using the inactive, passive side. Both active and inactive sides are tapered land type. The MR is directly coupled to the pinion of the gear box by a torsion rod, which has a high axial stiffness in comparison to flexible couplings. The purpose of this design feature is to reduce the axial thrust by the axial force of the single helical gear of the pinion.

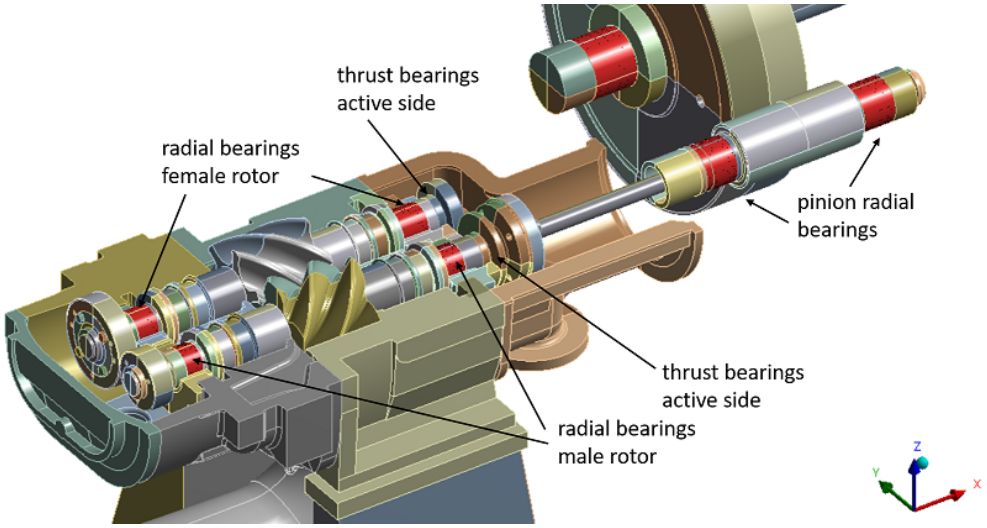

Figure 4: Bearing design of the screw compressor

The compressor design parameters are summarized in Table 1. The FGC MP 3rd stage compressor operates at 9250 rpm (154 Hz), has four (4) MR compressor lobes with a pocket passing frequency (PPF) of $4 \times 9250/60 \approx 617$ Hz; and a 2× MR speed harmonic at 308 Hz. The PPF and 2× harmonic are significant in this paper.

Table 1: Compressor design parameters

	LP Compressor	MP Compressor	
Process Stage	1st	2nd	3rd
Frame	SKUEL321L	CP200	CP160K
Gearbox	A35	B35	
Pressure (barA)	1.4–6.8	6.4–16.5	15–32
Flow rate (kg/h)	25000	50,000	
Molecular weight (kg/kmol)	50–53	30–36	28–34
MR Speed (rpm)	5828	7789	9250
Tip speed (m/s)	98	104	98
Power (kW)	1105	2836	

The three screw compressor models selected by the OEM had previous operating references at similar process conditions prior to this FPSO project. All three compressors were successfully tested in accordance with API 619 and ISO 1217 requirements at the OEM factory prior to delivery, with no indications of the high vibration issues experienced at site.

FIELD EXPERIENCES

First Operation

The compressors (LP and MP) were commissioned and put in operation in March 2020. The compressor operated intermittently until May 2020 accumulating approximately 215 hours. At that time, the compressors were only equipped with horizontal casing velocimeter for vibration monitoring. On 19th May 2020, FGC-MP 3rd stage casing vibration increased suddenly, and the compressor tripped on high vibration. A visual inspection of the third stage at site showed damaged rotors with severe scratches and wear on the profile surfaces. Consequently, the compressor was disassembled and shipped back to the OEM for inspection and repair. Both the FGC-LP-1st Stage and FGC-MP-2nd stage were in good order and no issues have been experienced with these compressors.

During inspection at the OEM, it was discovered the male rotor (MR) shaft had cracked at the thrust disk, allowing the rotor to move axially, causing the male and female rotors to come in contact, and the MR to contact the casing. The following observations were based on both visual and a detailed laboratory examination of the components: significant fretting wear at loaded flank of drive key and the shaft seat (Figure 6(a)), fretting damage on the shaft nut, several cracks at MR shaft under the thrust disk (Figure 6(b)). The largest crack passed 100% of the cross-section. Fatigue fracture with crack origin in key groove. Crack propagation due to torsional load. Damaged rotor surface caused by contact between rotors and the casing.

Analysis of the failure suspected a loose fit thrust disk and/or a torsional issue which may have contributed to the failure. A root cause was not determined at that time.

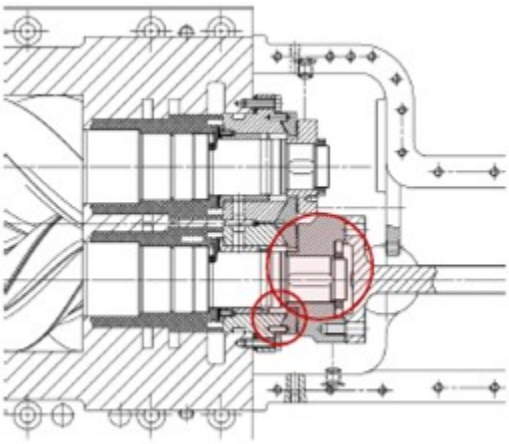

Figure 5: 3rd stage cross-section indicating observed damage areas

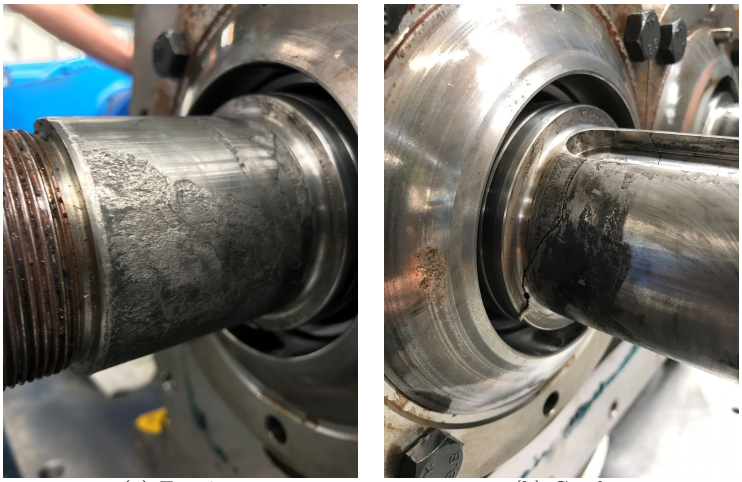

(a) Fretting (b) Crack

Figure 6: Damage on 3rd stage MR shaft under thrust collar

(a) MR (top) and FR (bottom)

(b) MR

Figure 7: Contact damage on 3rd stage rotors

2nd Operational Period Observations

The compressor was overhauled and returned to service. During commissioning and start-up, a vibration survey was carried out using handheld accelerometers and the single permanent casing accelerometer. Multiple vibration measurement points on and around the compressor were used - Figure 8. The vibration survey showed very high vibration during different compressor loading conditions. Most significant was a very high casing vibration in the axial direction on the compressor's timing cover (1.4 location) with a dominant 2× (308 Hz) component. It was also observed that the 2× component turned OFF, when the compressor discharge pressure dropped by several bar, and then it would turn ON with rising pressure. The 2× vibration component would also turn OFF with increased flow of the heavier LP (1st Stage) compressor gas to the MP Compressor (2nd and 3rd Stage) - Figure 9. The cause of the high vibration and the 2× phenomena could not be explained at the time. The compressor was removed from service and retrofitted with shaft radial and axial vibration probes to allow more enhanced testing.

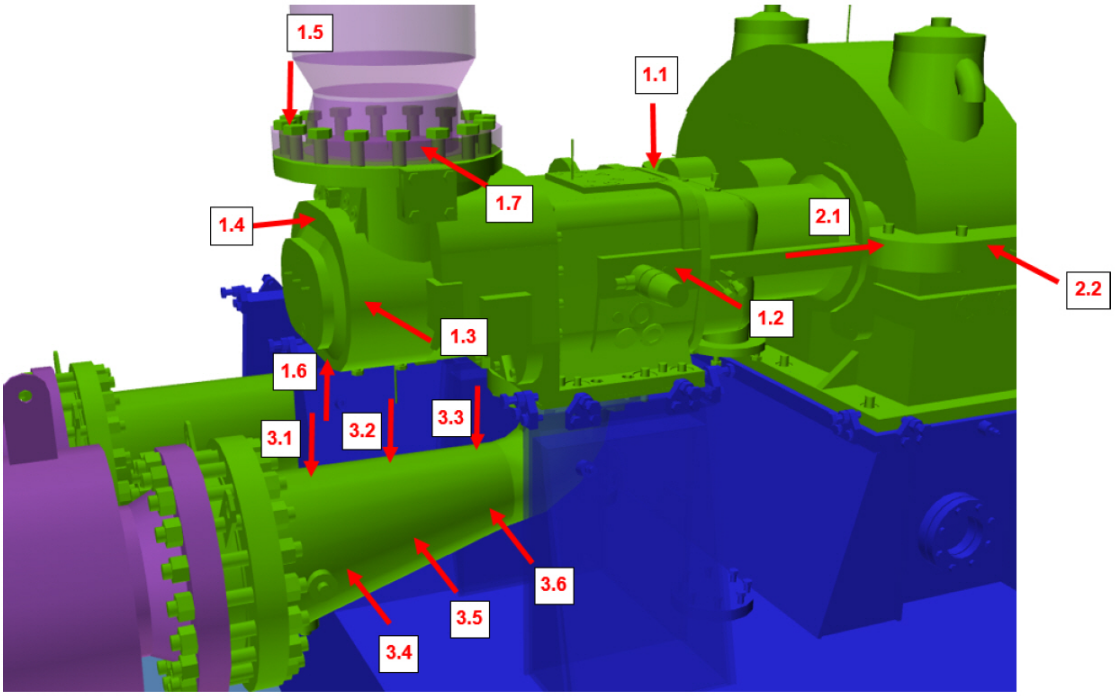

Figure 8: Casing and piping vibration measurement locations in the field

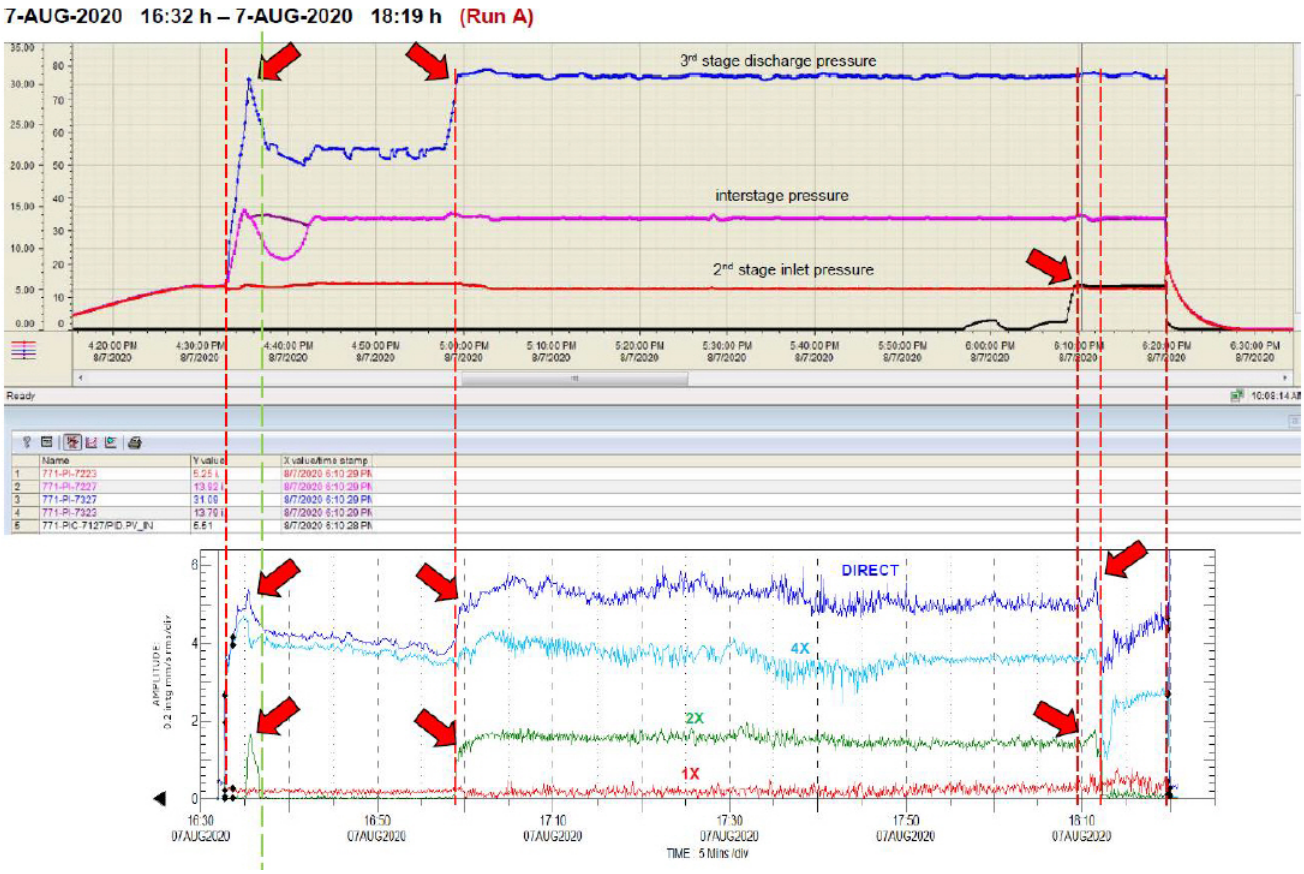

Figure 9: Vibrations versus operating conditions

Engineering Dynamics Incorporated
16117 University Oak, San Antonio, TX 78249
210-492-9100 www.engdyn.com

3rd Operational Period Observations

The compressor was returned to service with a third-party specialist contractor engaged to continuously monitor and gather high speed vibration and gas pulsation data. The compressor was tested for a range of different loading and gas compositions by adjusting flow rates from the LP and IP separators and adjusting compressor inlet temperatures. The most significant observation during the testing was the high vibration dominated by the 2× was the axial vibration of the MR. The MR radial vibrations were low. The FR radial and axial vibrations were also low. The high MR 2× vibration occurred at two (2) distinct operating conditions. During start-up, the onset of the high axial vibration was related to exceeding a certain differential pressure between suction and discharge. During normal operation, the onset of high axial vibration was linked to a shutdown of the LP compressor or reduction in flow from the LP compressor as shown in Figure 9. Additionally, during compressor coast down, there was observed a distinct axial resonance in the Bode plot (see Figure 10).

Figure 11 illustrates the onset of 2× axial shaft vibrations as operating conditions changed. At the beginning, the vibrations are steady (near 40 μm p-p) and dominated by PPF. When the vibrations increase slightly to approximately 45 μm p-p, *i.e.*, half of the thrust bearing's total end float (TEF) clearance, the vibrations suddenly grow in amplitude. Figure 11(b) shows these vibrations at this point are dominated by 2× or half the original PPF at 4×. Shown in yellow on Figure11(a), the MR shaft's position also appeared to shift approximately 10 μm at the same time the 2× vibrations are triggered.

Following the test program, the compressor was returned to service with a modified start and operational envelope to maximize the flow of the heavier LP gas to minimize compressor axial vibration. The MP compressor could be operated by maximizing the flow of higher MW gas from the LP Separator and reducing the amount of IP gas. Compressor casing vibrations were still relatively high, but not exceeding design trip limits. The compressor operated for approximately three months when it suffered a seal failure and rotor mechanical damage. The compressor was removed and returned to the OEM for inspection and analysis. The MR's suction side seal ring lock nut had loosened on the shaft causing the rotor to move axially and contact the female rotor.

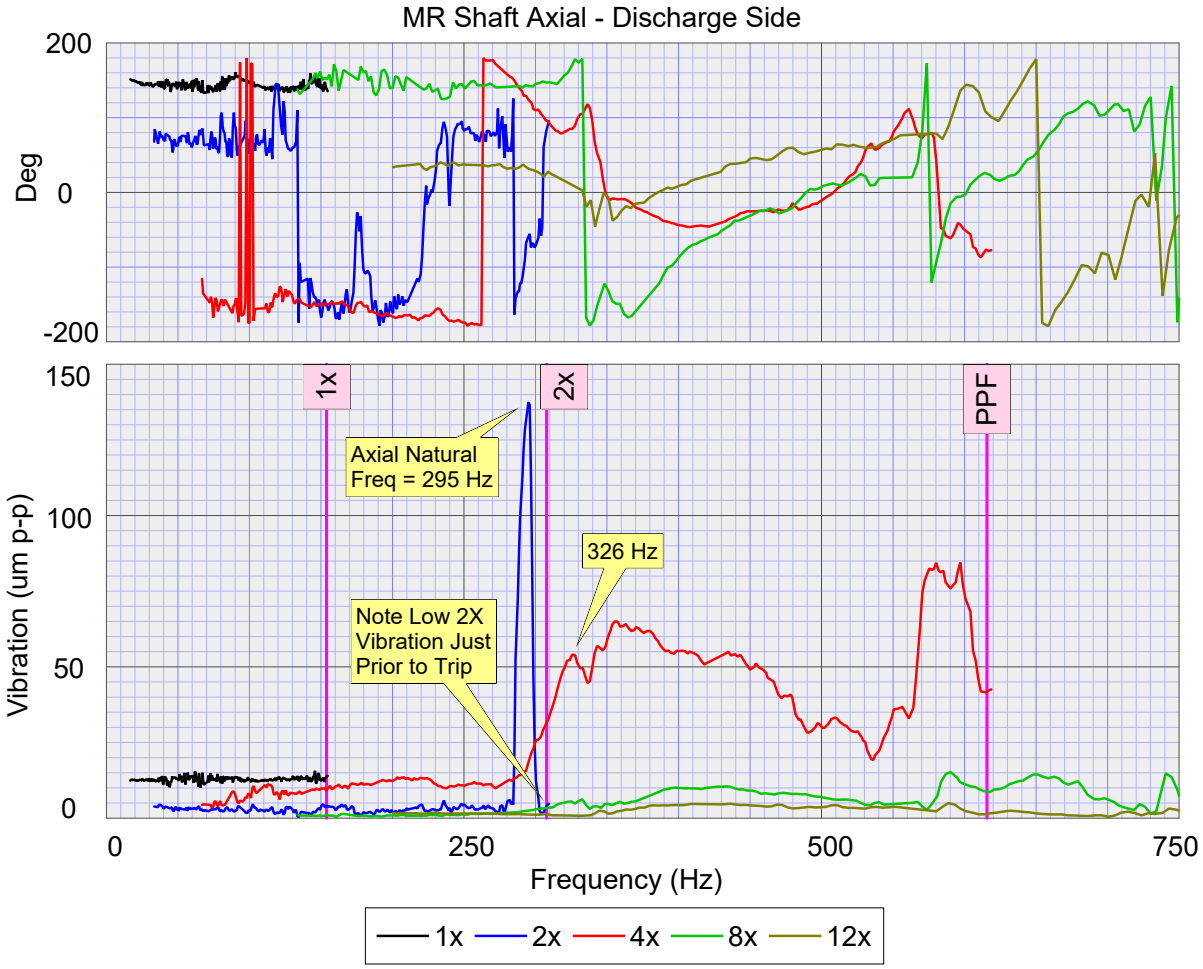

Figure 10: Axial vibration Bode plot during coastdown

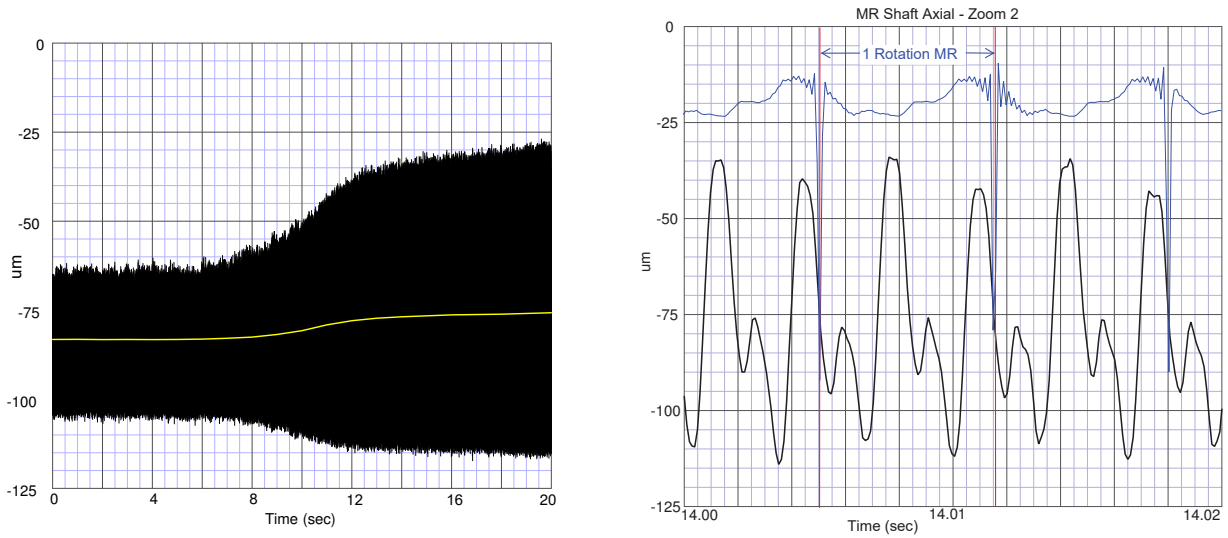

(a) 20 second timespan

(b) Zoomed waveform at 14 seconds

Figure 11: Measured MR shaft displacements showing the onset of 2× vibrations

4th Operational Period Observations

The compressor was again overhauled but this time several modifications were made to the compressor to shift the axial natural frequency. Thrust bearing clearance on the MR was reduced, thrust bearing contact surface reduced, thrust disk was modified to increase its mechanical stiffness. The compressor was returned to service and tested with the new configuration. There was no substantial improvement in vibration performance. Further optimization of operating procedures were implemented to maximize the Molecular Weight of the gas to reduce the MR axial vibration. Vibration levels continued to be high, limiting the operational envelope of the compressor.

5th Operational Period Observations

The compressor had experienced multiple discharge silencer failures since start-up. These failures are not covered in this paper, but one modification made to the compressor discharge venturi / pipe will be discussed here. The compressor discharge venturi was replaced with a pipe spool which included a resonator immediately on the compressor discharge flange (see Figure 12). This was the only change made to the compressor.

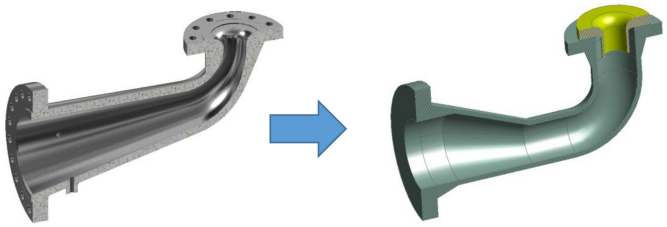

Figure 12: Modified discharge venturi with quarter wave resonator insert

On start-up and during testing, it was immediately apparent that the MR axial vibration and molecular weight interaction had changed. The compressor could not operate at the same gas through put and increased restrictions on the operational envelope of the compressor. The new venturi / resonator discharge pipe had improved the downstream acoustic pulsations, but it was detrimentally impacting the MR axial vibration (2×). This information provided significant insight to the main causal factor and final solutions.

Whilst the final compressor upgrade and factory testing progressed, the compressor was successfully operated for a number of months with continuous monitoring and adjustment of process parameters to maintain conservative axial vibration levels.

AXIAL DYNAMICS

Compared to lateral and torsional vibrations, relatively few axial vibration problems have been reported in the literature. Axial or "longitudinal" vibrations have long been of great concern in ship propulsion systems, given the lengthy shafting present [16]. Flow-related effects within tilting pad thrust bearings have been shown to cause subsynchronous axial vibrations [9] and, in some cases, these axial vibrations have coupled into problematic radial vibrations [19, 24]. High axial vibrations have also been encountered in electrical motors [35] and the structural dynamics of bearing pedestals have contributed to axial problems in turbo-generators [10, 34]. Recent experiences of axial vibration's negative effects on dry gas seal reliability [6, 17] have been the motivation for new axial vibration limits within industry standards for centrifugal compressors [2].

Compressor Modeling

In order to get a better understanding of the observed axial vibrations for the current problem and to find a solution to eliminate the high axial vibrations, a lot of effort was spent on simulations with regard to modal analysis. Early in the subject problem's investigation, a modal analysis of the MR string (MR, torsion rod and pinion) was carried out. In this analysis, mesh stiffnesses of the pinion gear and the timing gear were neglected, so that the rotor was supported in axial direction only by the oil film stiffness of the axial bearing. No interaction is considered between the MR and FR rotors as well between the MR and the casing through the journal bearings. The results in Figure 13 show the effect of oil film stiffness K_{act} on the first (1A) and second (2A) axial natural frequencies of the system.

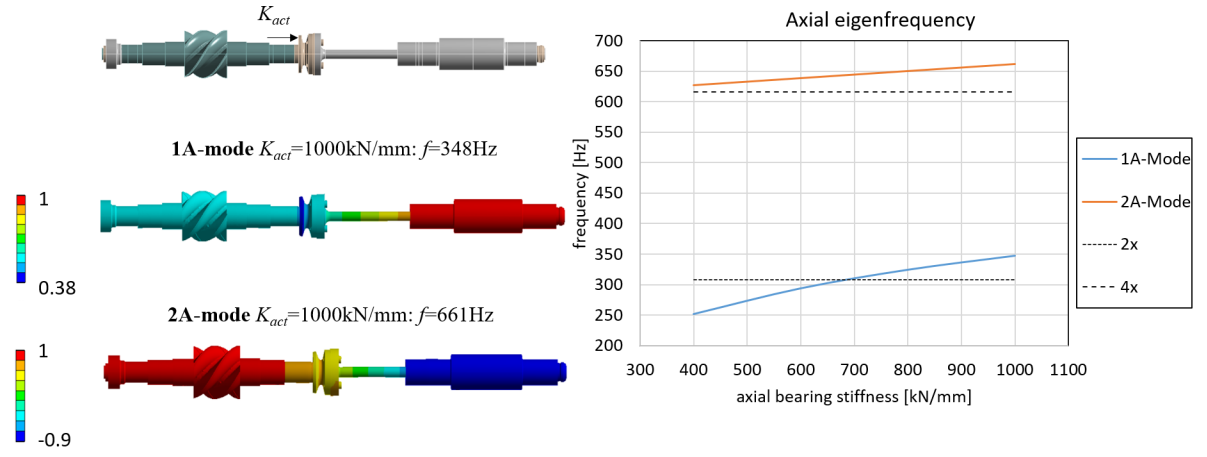

Figure 13: Modal analysis of MR string: Effect of oil film stiffness on the axial vibration modes

The 1A mode shown in Figure 13 is characterized by an in-phase vibration of both compressor MR and pinion against the oil film stiffness of the thrust bearing. Therefore, the location of its natural frequency is highly dependent on the oil film stiffness of the thrust bearing, which in turn depends on the axial static load on the bearing. In case of nominal thrust, an oil film stiffness of approximately $K_{act} = 1000$ kN/mm was calculated by means of a dedicated hydrodynamic bearing calculation program [21]. This yields an axial natural frequency of about 348 Hz, which is above 2× running speed.

However, based on the model simplifications made (the support stiffness of the bearing was assumed to be rigid, no interactions between other components) and the uncertainties in the calculation of the oil film coefficients, a reduced natural frequency towards a 2× excitation seems plausible. A reduced effective stiffness of approximately 680 kN/mm, would yield a frequency of 308 Hz equal to 2×, so that a resonance of the 1A mode with a 2× excitation was considered the most likely cause for the high vibrations.

The second eigenmode 2A is an out-of-phase vibration of pinion and male rotor, whose vibration node is located between both oscillating masses at the thrust bearing, and therefore increases only slightly with bearing stiffness. The eigenfrequency is always above 4× running as long as the bearing stiffness is above 30% of the calculated value of $K_{act} = 1000$ kN/mm. Therefore, the operation point was considered to be close to, but below the resonance condition. Thus, the elevated 4× vibrations were not a primary concern since they were expected for a screw compressor with four pocket pulsations per revolution and the amplitude measured at the bearing was still below the allowable limit.

To resolve the inaccuracies and for a better understanding of the system a detailed coupled lateral-torsional-axial model of the whole drive train is created for the understanding of the phenomenon. This comprehensive finite element model, shown in Figure 14, accounts for the following:

- Full 3D representation of the HP compressor drive train, including:

  - Compressor rotors and timing gear
  - Torsion shaft connection and gear box pinion
  - Thrust bearing spherical seat
  - Compressor casing
  - Base frame pedestals
  - Venturi
  - Suction silencer

- Thrust bearing oil-film stiffness is represented by distributed spring elements
- Radial bearings are modeled by bearing element connecting the rotor to the casing
- Mesh stiffness of gear box and timing gears, including the influence of helix and pressure angle of the teeth
- Bull gear, motor and 2nd stage compressor are represented as lumped masses to account for their overall contribution to the dynamic system

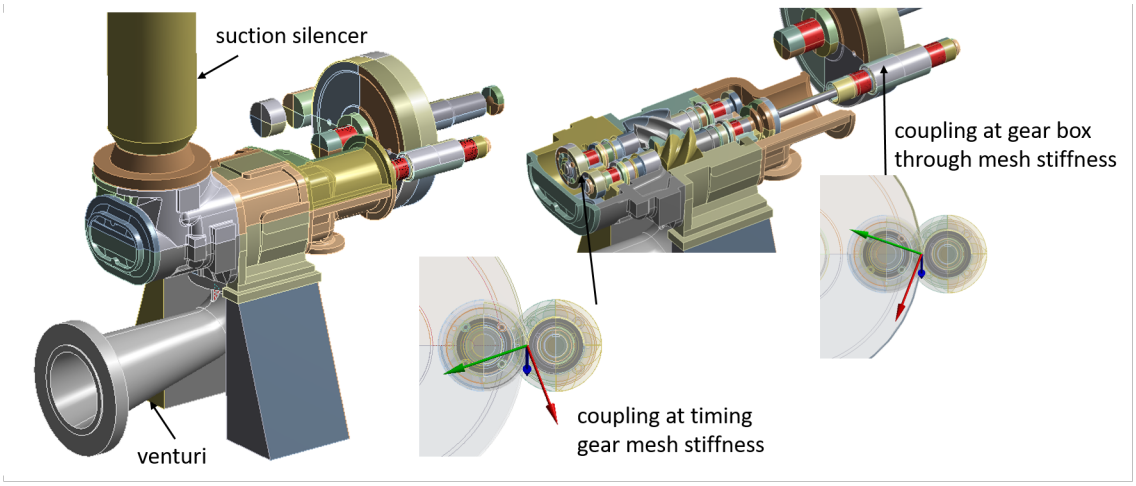

Figure 14: Coupled lateral-torsional-axial finite element model of the MP compressor train

A modal analysis based on this coupled lateral-torsional-axial model substantiates the assumption of the presence of an axial resonance near 2× excitation (Figure 15). Furthermore, the model is able to explain the observed apparent high utilization of thrust bearing clearance to a certain extent, as the additional flexibilities of the components, such as the spherical seat and thrust collar, contribute to higher measured relative displacements at the MR probe, which is attached to the casing and measures the relative displacement to the flange of the torsion rod.

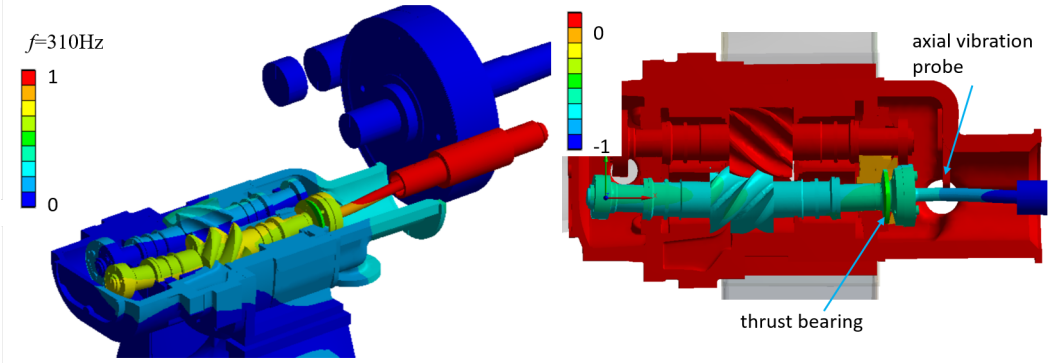

Figure 15: Overall (left) and axial displacement (right) of the 1A mode based on the complex FE-model of the MP compressor train: axial vibration of rotor and casing out of phase

Another important finding that could be obtained from the analysis of the coupled model was that there is only a weak coupling between the axial modes of MR string and the other components, such as the female rotor or the casing. Likewise, no significant coupled lateral-torsional-axial effects were involved. This confirms the validity of the simplified representation of the sub-string according to Figure 13 and, thus, allows an efficient further analysis of the phenomenon.

Even with this complex model, the observed phenomena could not be satisfactorily explained as a whole. Despite the obvious presence of a resonance situation near 2×, no clear cause for the excitation could be identified yet. Given the comparatively stiff torsion rod and the changing operating conditions made misalignment excitation, generally associated with a 2× excitation, a possible cause for the observed vibration phenomenon. Nevertheless, excitation by misalignment at this level seems unlikely, especially since the alignment was checked several times and carried out accurately. Furthermore, the 1A mode is characterized by main displacements in the hydrodynamic bearings and, therefore, expected to be relatively well damped. This does not match with the sudden occurrence of 2× vibrations with an extremely high amplification factor, in addition to the 4× vibration.

Nonlinear Modeling Approach

Based on the new measurements during the 4th and 5th testing campaign and the knowledge gained here, an extended non-linear theory of the vibratory system was developed. The starting point for this theory were two observations:

- An apparent static shift of the thrust collar displacement at the onset of 2× vibrations according to Figure 11(a)
- High level of 2× axial vibrations was measured (with double amplitudes in the range of the total end float clearance) without the presence of significant 2× axial excitation.

Previously, the bearing calculations were carried out for the design operation point based the nominal thrust. To obtain the stiffness and damping coefficients, oil film forces and displacements were linearized around this point. At these high vibration amplitudes, with the use of almost the entire bearing clearance, it becomes obvious that a linearization around the operating point is not suitable to describe the reality.

Therefore, quasi-static bearing stiffness coefficients are derived for different oil film thicknesses on the active and passive side by COMBROS-A [21], a journal bearing calculation program for non-isothermal calculation of static and dynamic bearing characteristics of hydrodynamically lubricated thrust bearings. The oil film thickness is varied between 1 μm and 90 μm to cover the whole range of the axial bearing clearance. The program calculates the equilibrium condition and pressure distribution within the oil film and provides the static bearing load as well as stiffness and damping coefficients.

The total load-displacement curve is obtained by the superposition of the individual quasi-static stiffnesses of the active and passive side for all calculated oil film thicknesses (Figure 16). The oil film reaction force increases progressively for small oil film thicknesses, yielding a high momentary stiffness for large deflections towards the total end float. In between, the stiffness is significantly lower.

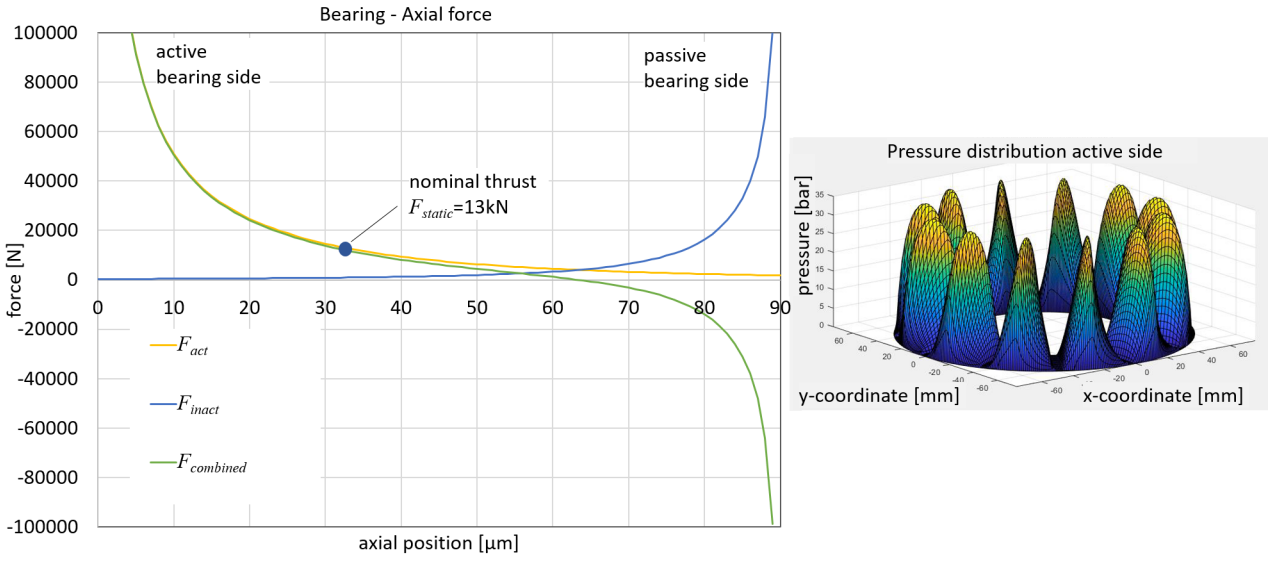

Figure 16: Active and inactive thrust bearing oil film forces vs. thrust collar position along with example oil film pressure distribution at active side for normal thrust load

The non-linear approach allows to explain the measured sudden change of axial position of the male rotor in operation, which correlates in each case with the onset of very high 2× oscillation (see measurements in Figure 11). Unlike before, this displacement is not regarded as a quasi-static overall displacement caused by increased discharge pressure and power. In the context of the extended non-linear oscillator theory, this displacement can rather be considered as a shift of the mean value of the vibration signal (Figure 17), caused by the non-linear motion in the oil film with non-symmetrical axial stiffness. At the design operation point, the oil film thickness on the active side of the bearing is smaller than the one on the inactive side. At small vibration amplitudes, the oil film can be described by a linearization around the design point yielding vibration amplitudes in both directions. However, when the rotor vibrates at large amplitudes, the deflection increases mainly towards the inactive, passive side. As a consequence, the mean value in the transient measurement signal changes. Thus, the observed shift in axial position of the rotor is not caused by a change in thrust, but rather by the large vibration in combination with the non-linear characteristics of the bearing.

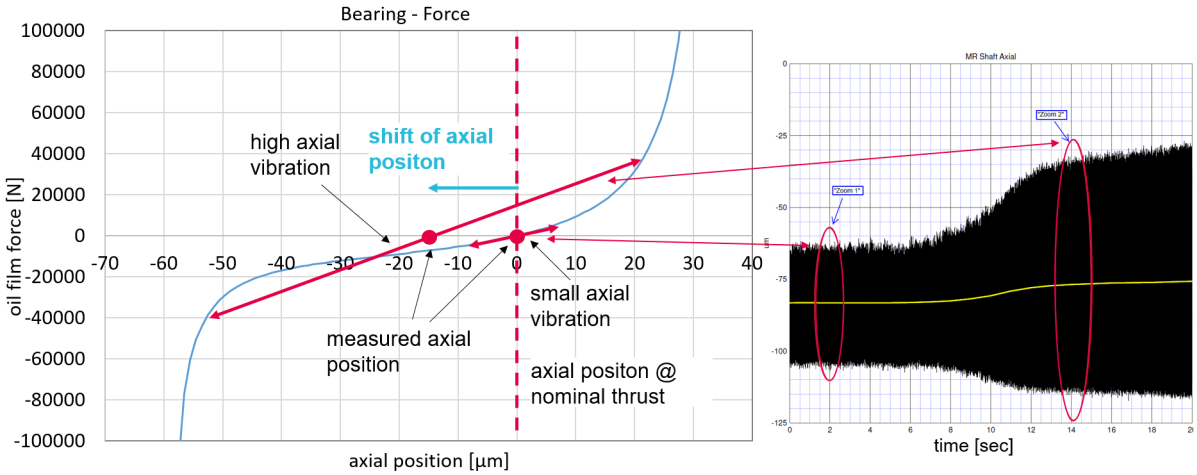

Figure 17: Correlation between axial vibration amplitude and mean value as apparent quasi-static axial displacement

This new finding indicates that the particular vibration characteristic observed here is mainly influenced and described by the large axial movement or vibration using nearly the full bearing clearance. This makes it evident, that the axial stiffness can no longer be represented by a linear spring, *i.e.*, by a simple stiffness coefficient, but rather as a non-linear function of the position and restoring force as shown above.

Non-linear vibration phenomena are also discussed in literature with practical relevance. In [11], it is stated that the non-linear characteristic curves of hydrodynamic bearings, as is the case here, can be the origin of the subharmonic resonances in rotor dynamic problems.

For such a nonlinear oscillator and in contrast to a linear representation, the response and its frequency is dependent on the level of the excitation amplitude. This observed and so called "period doubling" bifurcation phenomenon is a typical characteristic for nonlinear oscillators.

In case of a linear system excited by a harmonic force of the frequency ω, the structure will always oscillate with the same frequency ω as well. On the contrary, for a nonlinear system, the frequency component of the vibration will not always be equal to the frequency of the external force. Instead, different types of resonance can occur, such as the subharmonic resonance, superharmonic resonance, or a combination resonance for multi-degrees of freedom systems [11, 23]. In the case of a subharmonic resonance (SHR), the frequency output is equal to a fraction of the forcing frequency, i.e., ω/n where n is an integer).

A typical representative of non-linear oscillators is the oscillator investigated as early as 1918 by the German engineer Georg Duffing (1861-1944) (and named after him) [12]. This well-known example is often used to reveal that a large variety of dynamic motions can occur in nonlinear simple systems [3, 5, 20, 23]. It can be regarded as an extension of the harmonic oscillator, which is based on Hooke's linear law, by a cubic restoring force hence a nonlinear elasticity.

In summary, the following characteristics emerge for a general non-linear oscillator with primarily non-linear stiffness behaviour:

- Response with subharmonic response of an integer fraction of the forcing frequency
- Sudden onset of subharmonic response (jump phenomenon)
- High response amplitude

Early studies of this SHR phenomenon focused on strings and laminated materials [22] and were observed on aircraft with reciprocating, internal combustion engines [32].

This phenomenon has been reported on relatively few occasions in the rotordynamic community. SHR caused high lateral vibrations on a turborotor supported by gas-lubricated, foil bearings [31] and on a steam turbine during a blade loss event [1]. In the rotating machinery field, probably the most well-known instances of SHR or "fractional-frequency rotor motion" are those encountered in aircraft engines where nonlinear effects due to stator rubs, rolling element bearings, and squeeze film dampers occur [8, 14, 15].

Even though the potential for *axial* SHR has been predicted [33], no previously published field experiences could be identified. A case history [13] involving large boiler fans may have experienced a similar phenomenon, but their axial vibration issues may be more related to lateral-axial coupling effects.

Based on the discussions above, a simplified lumped mass model of the active thrust bearing and the rotor assembly was established in order to confirm the non-linear theory in the present case (Figure 18). The lumped mass oscillator exhibits a natural frequency at 308 Hz, representing one half of PPF or 2×. The oil film is modelled by the load displacement curve (Figure 17) in which the force of the oil film on the rotor is a non-linear function of the axial position. However, the damping values were reduced in order to promote the phenomenon. The rotor is excited by a harmonic excitation with a frequency of 4× running speed.

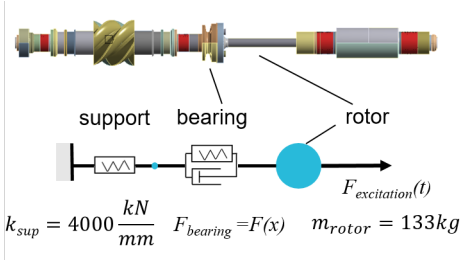

Figure 18: Simple lumped mass oscillator with non-linear stiffness representation (support stiffness k_{sup} derived from harmonic analysis)

Simulation results are shown in Figure 19. The simulation is started with an excitation force of ±1000 N (about 8% of the nominal thrust) for 500 ms to reach a steady state. The resulting response is small, as the 4× excitation is well above the natural frequency of the linearized lump mass model of about 308 Hz. The phase shift of 180°, which is characteristic for an operation above the critical speed can be seen in the zoom of the time signal, then the excitation is linearly increased. At the beginning, the rotor responds with increasing amplitudes. However, once a sufficiently high level of 4× (PPF) axial excitations of 15 kN is reached, the nonlinear phenomenon of SHR or "period doubling" occurs suddenly as described above, which results in high 2× axial vibrations as shown in Figure 19.

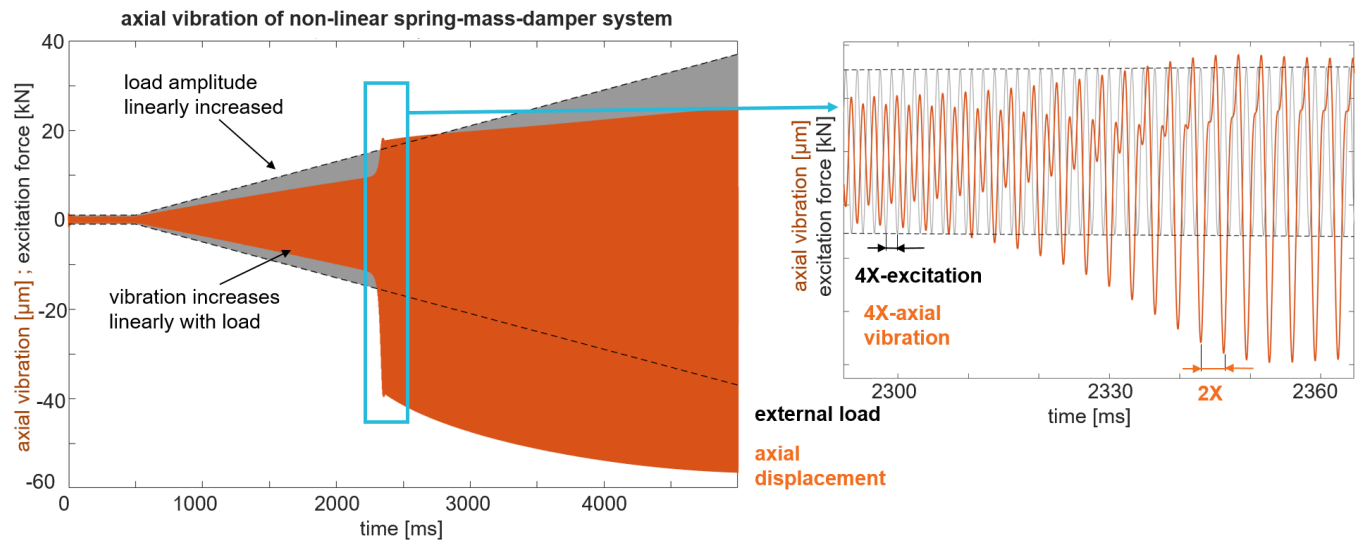

Figure 19: Predicted sudden occurrence of SHR phenomenon with 2× response due to pure 4× excitation

Engineering Dynamics Incorporated
16117 University Oak, San Antonio, TX 78249
210-492-9100 www.engdyn.com

Sensitivity studies were carried out using this simple model showing that besides a high 4× excitation, a necessary condition seems to be a certain sensitivity for an oscillation at 2× (which is given by the presence of a 2× axial natural frequency or the male rotor). Furthermore, the phenomenon of the transition to non-linear vibrations was directly related to the amount of damping that was considered in the oil film. The onset of SHR vibrations shifts towards higher excitations forces with increasing damping.

In conclusion, the simple lumped mass nonlinear model allows to understand the given period doubling vibration phenomenon and to explain other observations in the same context, such as the sudden onset and the apparent shift in axial position. It requires only small changes in the excitation force to trigger the sudden change in vibrational behaviour as described by the non-linear theory. A change in gas parameters may cause this change in excitation force.

Nevertheless, there are still some inconsistencies and limitations. Realizing that the non-linear characteristic of the oil film is only relevant for high vibration amplitudes, the second axial mode (2A) (Figure 13) has to be taken into account. The proximity of the second eigenfrequency to the given excitation at 4× running speed yields an elevated level of vibrations. This condition, in combination with the special ratio of first and second natural frequency of about two seem to make this rare phenomenon in fact possible. To gain a further understanding, an extension of the rotor model from a lumped mass to a more detailed representation of the string is necessary. Additionally, the approach to describe the non-linear characteristics of the oil film by a quasi-static analysis only approximates the actual dynamics in the oil film. In particular, the damping values may be overestimated.

To eliminate some of limitations of the simplified analysis and help gain confidence in SHR candidate theory, a higher fidelity nonlinear analysis was performed. Figure 20 presents the rotor assembly model of the compressor MR, torsion shaft and pinion developed for this more detailed simulation.

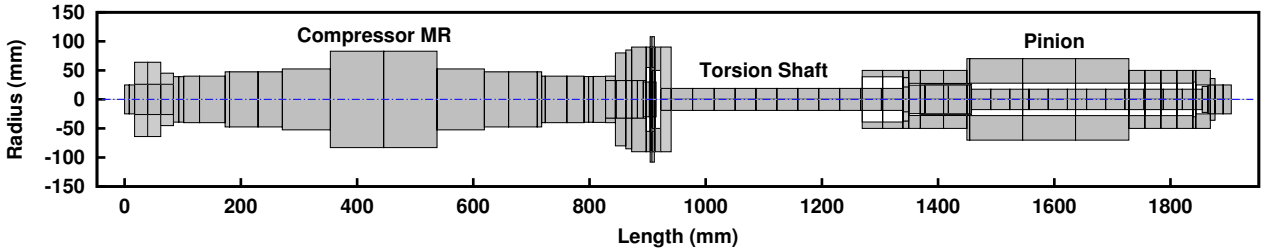

Figure 20: Model of rotor assembly

To address the expected flexibilities within the thrust bearings' supporting structure, the simple, two degree of freedom model shown in Figure 21 was implemented. The mass of the active bearing's spherical thrust ring is supported by K_{RING} which is backed by the bearing housing mass and its stiffness K_{HSG}. Both of these stiffness estimates were derived from a detailed FEA of the compressor's assembly. Displacements and velocities of the thrust ring and bearing housing relative to the rotor's thrust collar and splash ring are important inputs for the modeling of the active and inactive thrust bearing oil films.

The nonlinear, transient oil film forces (F_{act} and F_{inact} in Figure 21) produced by the active and inactive bearings were calculated using a 2D finite element solution of Reynolds equation [18]. This solution considered the hydrodynamic pressure generated from shaft rotation as well as squeeze effects due to relative motions between the shaft and bearing housing/thrust ring. Variable viscosity and starvation effects were also included.

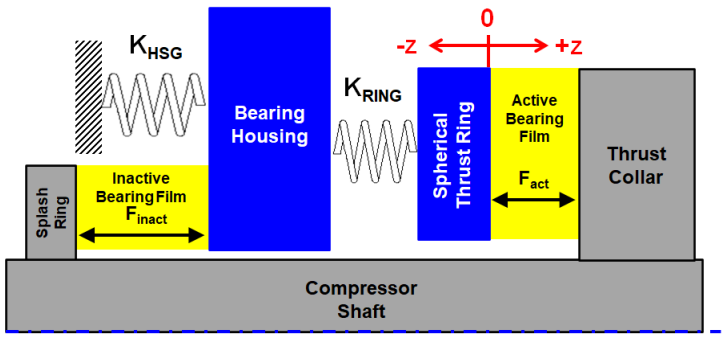

Figure 21: Thrust bearing housing model for nonlinear axial simulation

Such nonlinear analysis of fluid film thrust bearings has received some attention over the last 20 years [4,28,36]. However, much of it has focused on thrust bearing effects on lateral vibration, not axial, such as several recent investigations on automotive turbochargers [7,26].

The system was assembled together with the rotor and bearing housing models dynamically coupled together only through the thrust bearings' oil film forces. Time transient simulations of the system were done using the fourth order Runge-Kutta technique. Given the high frequencies of interest, a very small time step of 2 μs was required. Axial displacements z and velocities $\dot{z}$ of all rotor system degrees of freedoms and two bearing housing masses were calculated due to two specified, constant forces on the compressor: the static thrust load F_{static} and the PPF excitation force at $F_{4\times}$.

Figure 22 shows the predicted axial vibrations at the MR probe location for two different static thrust loads and 6 steps of increasing pulsation force magnitude. Examining Figure 22(a) with rated static thrust load, the response increases slightly as expected for each increase in $\|F_{4\times}\|$ and remains constant over the approximately 0.15 s period until the next pulsation force increase. There is no growth of response that is not due to an increase in pulsation force magnitude, even when the vibrations reach approximately 55 μm p-p or 68% of the TEF. The frequency of the vibration remains the same as the excitation's, *i.e.*, PPF or 4×.

However, Figure 22(b) shows a dramatic increase in response occurs under a static thrust load of 125% rated. Specifically, such rapid growth seems to be triggered when the $\|F_{4\times}\|$ causes approximately 45 μm p-p in response. One can observe this behavior in Figure 22(b) from the period of time from 0.55 s to 0.7 s, when the overall response grows from approximately 45 μm p-p to approximately 70 μm p-p. After this point, there are no further increases in response without a corresponding increase in pulsation force.

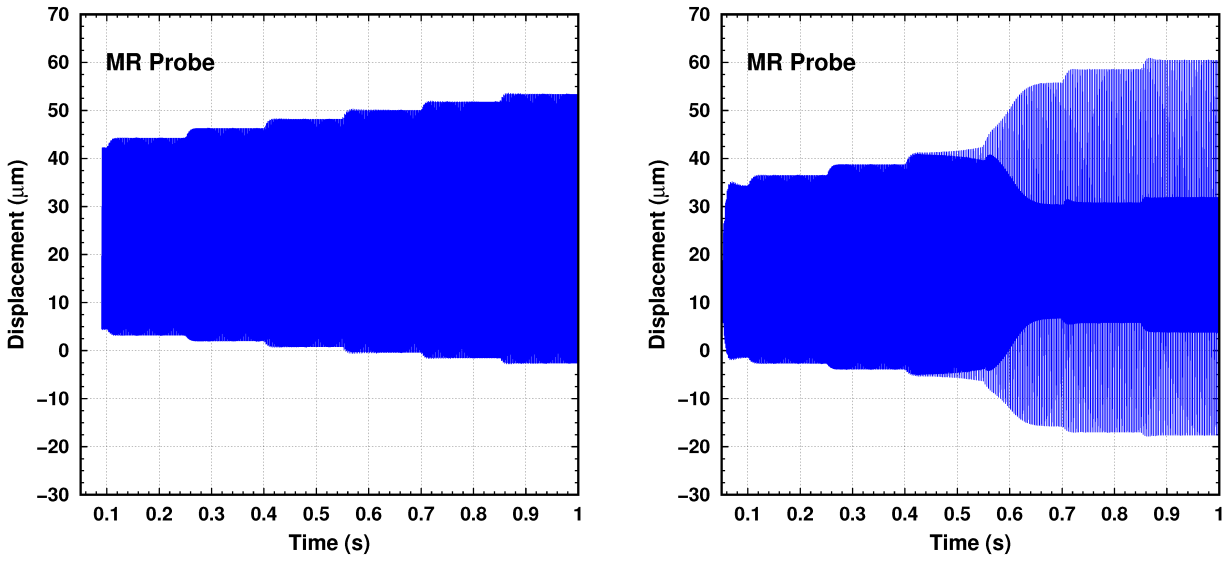

(a) F_{static} = 100% rated

(b) F_{static} = 125% rated

Figure 22: Predicted shaft axial displacements at MR probe with increasing $\|F_{4\times}\|$ for different static thrust loads

Figure 23 presents the axial vibration's frequency content for the 125% thrust load simulation (Figure 22(b)). Prior to approximately 0.55 s, the response is solely at 4× due to the pulsation force applied. However, when the $\|F_{4\times}\|$ is increased to approximately 8000 N (1800 lbf) 0-p at 0.55 s, a second frequency component at 2× appears, grows, and then stabilizes in amplitude before the next pulsation force increase at 0.7 s. This 2× vibration is triggered when the vibrations reach approximately 45 μm p-p, a behavior that correlates well with the field measurements shown in Figure 11.

Figure 23's 2× amplitude of 33 μm p-p is significant (*i.e.*, nearly half the TEF), yet, it remained well below the observed levels in the field. In a linear sense, the actual machine appeared to have less stiffness or damping that was allowing for greater response. Simulated starvation of the inactive thrust bearing produced higher vibration levels, however, oil flow measurements ruled out starvation as a contributor. While the under-prediction of vibration levels suggested an unknown physical mechanism was likely unmodeled, this was not considered a vital discrepancy given the recognized modeling uncertainties and the reasonable correlations with measurements.

The predicted initiation of vibrations at half the PPF helped confirm SHR as the likely problematic behavior observed in the field. The simulations agreed with field experience that the 4× vibration had to be sufficiently large enough (a little over 50% of the thrust bearing's TEF) to initiate the subharmonic 2× vibrations. As such, efforts began to focus on the factors contributing to the relatively large 4× vibration.

Although the 2A mode's close proximity with PPF was likely contributing, per Figure 13, this mode's frequency was not expected to change with operating conditions like the 4× vibrations were observed to do. Changes in process gas composition had been shown to alter the 4× vibration in the field. Therefore, it was hypothesized that acoustical (pulsation) effects, rather than the 2A mode's proximity, were the dominant factor controlling the 4× vibration amplitude.

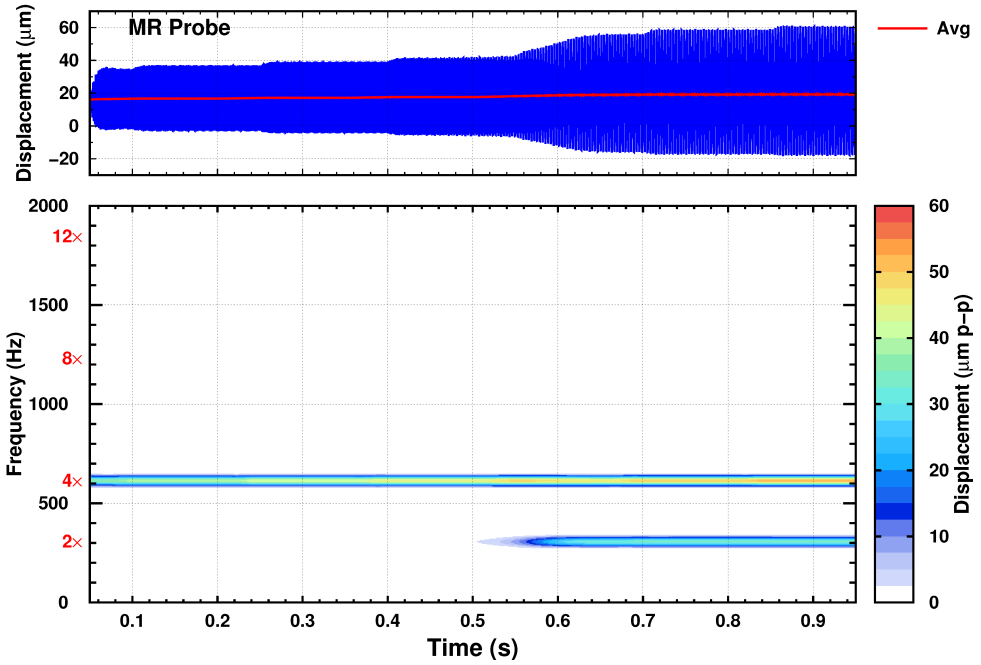

Figure 23: Frequency content for MR probe displacements at $F_{static} = 125\%$ with increasing $\|F_{4\times}\|$

PULSATION DYNAMICS

For screw compressors, energy is dissipated by mechanical effects, flow noise, and gas pulsations [25] generated by the compression process. Since the gas pulsation frequency produced by these compressors and the problematic vibration frequency was the same, pulsation induced shaking force from the compression process was the likely primary excitation source.

Pulsation Generation in Screw Compressors

A screw compressor is a positive displacement machine like a reciprocating compressor. Instead of a piston in a cylinder, a screw compressor utilizes two counter-rotating intermeshing rotors that trap a volume between the case and the outer portion of the "screw". As the screws rotate, the trapped pocket of gas transfers axially, reducing the physical volume of the gas passage. At some point in the rotation, a port is exposed at the discharge of the compressor, releasing a pulse of gas into the process. This unsteady flow results in pulsation generation. Many factors affect the magnitude of pulsation, including the screw profile, internal clearances, shape of the discharge port, and the internal volume ratio (V_i) [29].

The V_i is defined as ratio of the volume of gas when initially trapped (V_s), to the volume when the discharge port is exposed (V_d). Since the pressure ratio across the machine (P_i) can be defined as the ratio of discharge pressure to suction pressure, the following relationship can be obtained.

$$P_i = V_i^k \quad \text{or} \quad V_i = P^{\frac{1}{k}}$$

where: k = specific heat ratio of the gas
$= \dfrac{c_p}{c_v}$ for ideal gases

Each machine has a characteristic V_i determined by internal geometry. For a given set of operating conditions, the process V_i may not match the machine V_i, resulting in either over- or under-compression. The result is an increased outgoing flow pulse amplitude for over-compression or an inward flow pulse from the process in the case of under-compression, resulting in higher generated pulsation amplitudes.

For many screw compressors including this one, the geometry of the meshing rotors produces 4 pockets per revolution of the drive rotor (PPF). This mechanism results in pulsation primarily at integer multiples of 4× running speed. Oil-free screw compressor operating speeds are necessarily rather high to overcome internal leakage and achieve the desired flow rates. For this case of 9250 RPM, the compressor will generate pulsation at 617 Hz, 1233 Hz, ...

Amplification

In addition to mechanisms that generate pulsation, acoustical natural frequencies (referred to here as GNF for Gas volume Natural Frequency) of the machinery cavities and piping can dramatically increase the amplitude of pulsation. A GNF is a condition where pressure waves traveling in a medium interfere constructively, resulting in amplification of the pressure wave. For one-dimensional acoustics, the standing wave that is produced has a wavelength (λ) enforced by the particular boundary conditions of the medium. For example, in a closed-ended space such as piping, a GNF will exist when $\lambda = \frac{2L}{n}$

where: L = characteristic length (m)
n = 1,2,3,...

The wavelength of a sound wave at a particular frequency is the speed of sound (c) divided by frequency (f) expressed as $\lambda = \frac{c}{f}$, so the family of GNFs for this closed-closed pipe (often termed a "half-wave") can be calculated using the expression

$$f_n = n\frac{c}{2L}$$

where: n = 1,2,3,... (fundamental and integer harmonics)
f_n = n^{th} natural frequency (Hz)
c = speed of sound (m/sec)

When the GNF is coincident with PPF, high amplitude pulsation can result at that frequency. This condition is known as an acoustical resonance. In many screw compressor discharge cavities, the geometries and excitation are such that system acoustics can be three-dimensional as well as one-dimensional [27]. For this machine, the characteristic lengths of the GNFs inside the compressor cavity and piping were in the range of the wavelength of the excitation, which caused acoustical resonances and high amplitude pulsation that resulted in excessive vibration at PPF.

Speed of Sound Effects

In a constant speed machine, PPF excitation is constant. It would seem unusual for PPF excitation to exactly match a GNF. However, changes in speed of sound of the process fluid will change λ, thereby shifting the GNF. Molecular weight (MW), temperature, and to a lesser degree pressure will alter the speed of sound, potentially resulting in acoustical resonance with PPF excitation. This behavior is illustrated in Figure 24. Constant speed PPF energy can excite several of the GNFs as they shift left or right depending on the speed of sound. This behavior explains why excessive vibration in the field could be reduced by altering the temperature and gas composition.

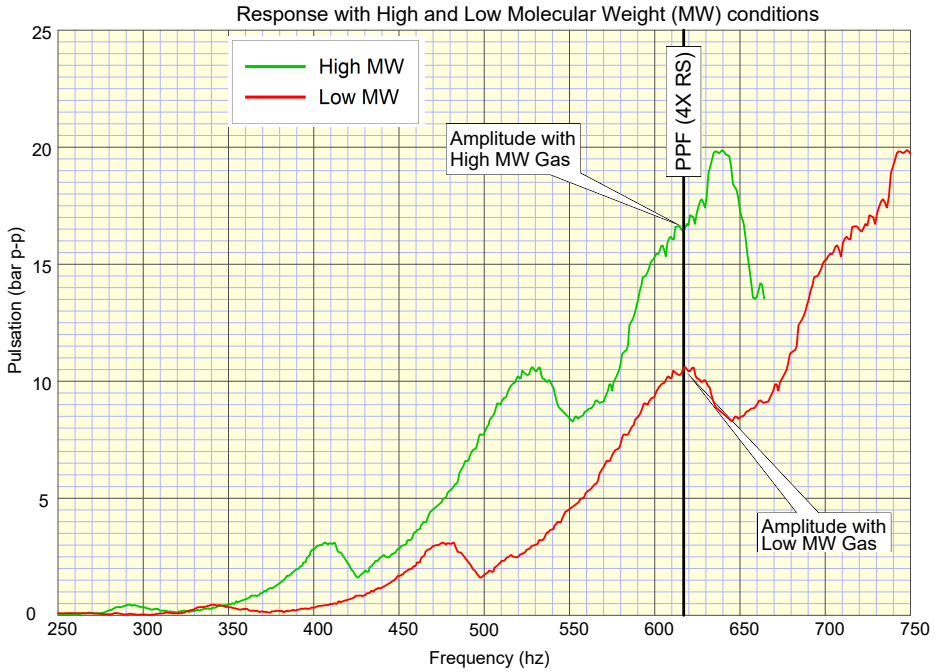

Figure 24: Comparison of potential response to PPF at different gas conditions

DESIGN MODIFICATIONS / MITIGATIONS

Modifications were developed to reduce the axial vibrations by changing rotordynamic design. The compressor cavity was also altered to reduce pulsation amplitudes. As these modifications were implemented, enhanced factory acceptance tests (EFAT) were conducted to determine their efficacy.

Rotordynamics

The final design modifications to the rotating equipment of the compressor are outlined in Figure 25, which compares the original arrangement to the ultimate design. Rotordynamic analysis predicted that replacing the 3rd stage torsion shaft by a standard coupling would resolve the 2× axial rotor vibration issue. To effect this modification, the torsion shaft was replaced by a standard flexible element coupling, which is less rigid in the axial and lateral directions. This change required the axial bearings to be completely altered. The original male rotor tapered land thrust bearings were replaced by tilting pad bearings to increase the axial stiffness and to counteract the higher loads that resulted.

In the original configuration, the torsion shaft transmitted torque from the pinions to the compressor rotor. This configuration fixed the pinions at their axial position and compensated the axial thrust generated by the single helical gear. Since the new coupling was not able to transmit axial forces, the gear design was changed from a single helical to double helical. However, this change also required the second stage pinion to be double helical, which necessitated a new coupling thrust disc for that stage.

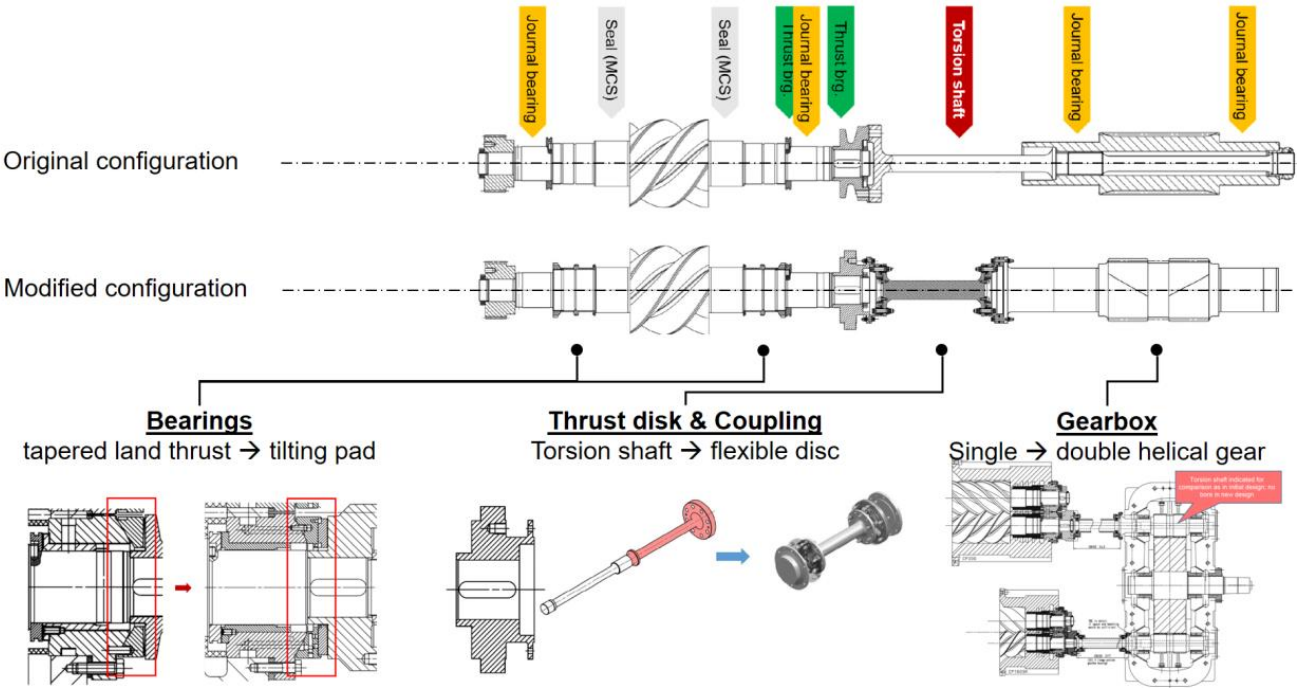

Figure 25: Final design modifications of rotating equipment

EFAT - Pulsation (Acoustical) Data

A test stand was constructed at the OEM shop for string testing of the compressor. Because of the short wavelength of pulsation, insertion probes [27] were necessary to obtain accurate pulsation data. Similarly, it was necessary to machine additional measurement ports to the compressor case.

For safety reasons, CO_2 gas was used instead of process gas. While this gas had similar acoustical properties to the process gas, the full range of speed of sound (SOS) expected in the field could not be tested. Calculations of all expected gas compositions showed that SOS could vary from 280-345 m/sec, corresponding to a λ change of 0.45 m to 0.56 m.

Some change in speed of sound could be accomplished by changing the temperature of the CO_2, but this was still less than the range expected in the field. To overcome this limitation, the compressor was operated at different speeds. Reducing the speed increased λ and vice-versa. In this manner, the full range of λ could be obtained using a single gas, simulating a full range of speed of sound in the field. The data acquisition system computed λ at a particular instant by continuously calculating the speed of sound at the current temperature and pressure, then dividing by the current PPF. After adjusting

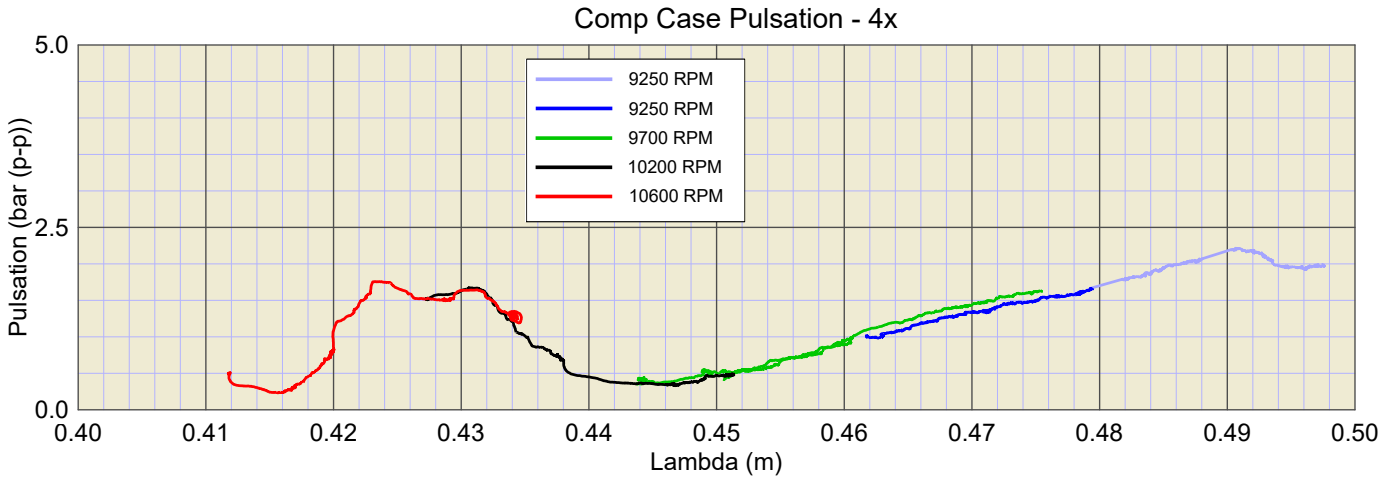

Figure 26: Pulsation amplitude versus λ plot

for speed of sound differences between the modeling and the test stand and scaling for static pressure differences, the data were plotted versus λ.

Figure 26 presents measured pulsation data versus λ. The various line colors indicate a speed and temperature range that was used on a particular test series. Combined, they represent the full range of testing. This plot has the horizontal axis reversed from the usual sense of amplitude versus frequency, however for later comparisons with analytical results, the data were re-plotted versus frequency.

3-D Acoustical Analysis

A three-dimensional model of the compressor discharge cavity and the downstream piping was developed using the ANSYS FEA code. It was quickly determined that the results were sensitive to the cavity volume at the discharge of the compressor, including volume in the exposed flutes of the meshing rotors. Using the geometry of the rotors [30], their volume was determined and was removed from an empty compressor volume to get the fluid volume shown in Figure 27.

The upper and side volumes were then deleted to give the total discharge compressor volume. This was done at 15° increments of male rotor rotation until the best agreement to field data was obtained, resulting in the volume shown in Figure 28.

Data from the test stand with the original system was used to normalize the model. For comparison to the ANSYS results, the data were plotted versus frequency, instead of lambda. One such comparison is shown in Figure 29. The light grey trace in Figure 29 is the normalized FEA model response predictions, while the (red) and (green) traces depict test stand data.

Shifting a GNF in frequency could result in a system free of GNFs over the range of operating conditions. Using the 3-dimensional acoustical model, the diameter, length, and shape of the internal flow path was adjusted repeatedly to optimize the acoustical response characteristics — i.e., the acoustical natural frequencies were spread apart and shifted to be out of the range of potential 4× excitation, thereby avoiding a resonance condition. Although a very complex shape could have resulted from the optimization efforts, the resulting internal shape was essentially a smooth pipe, with a 1/4-wave resonator at the entrance to the discharge venturi.

The analysis with this geometry predicted that the GNF would move lower in frequency with the mode shape shown in Figure 30.

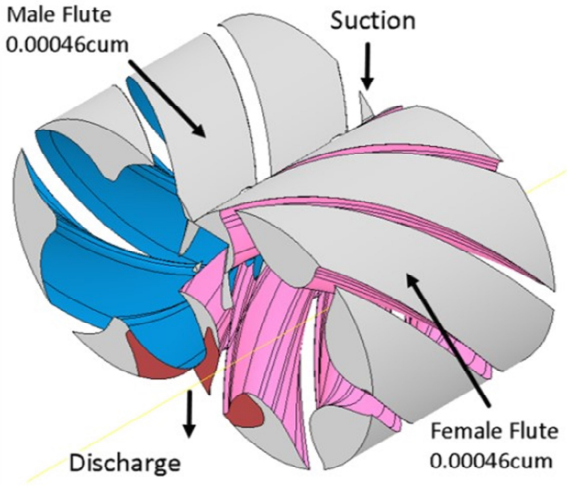

Figure 27: Compressor rotor volume – all flutes

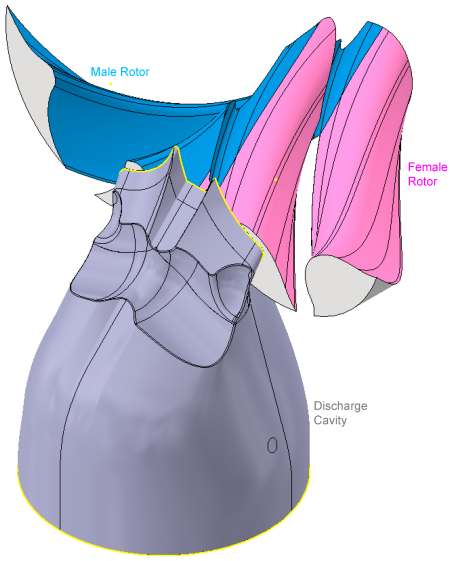

Figure 28: Discharge volume at 30°

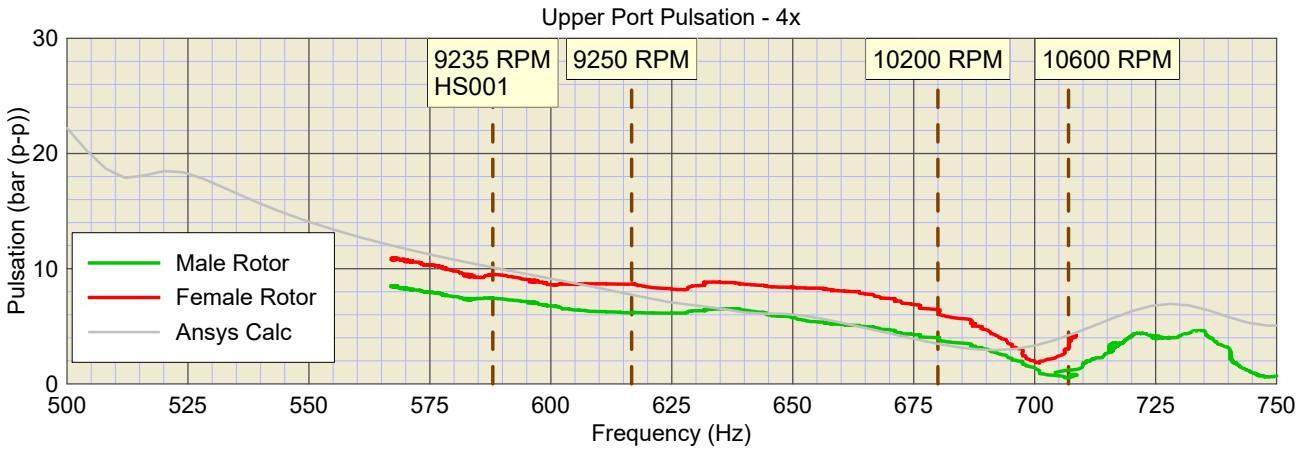

Figure 29: Comparison of analysis and test stand data

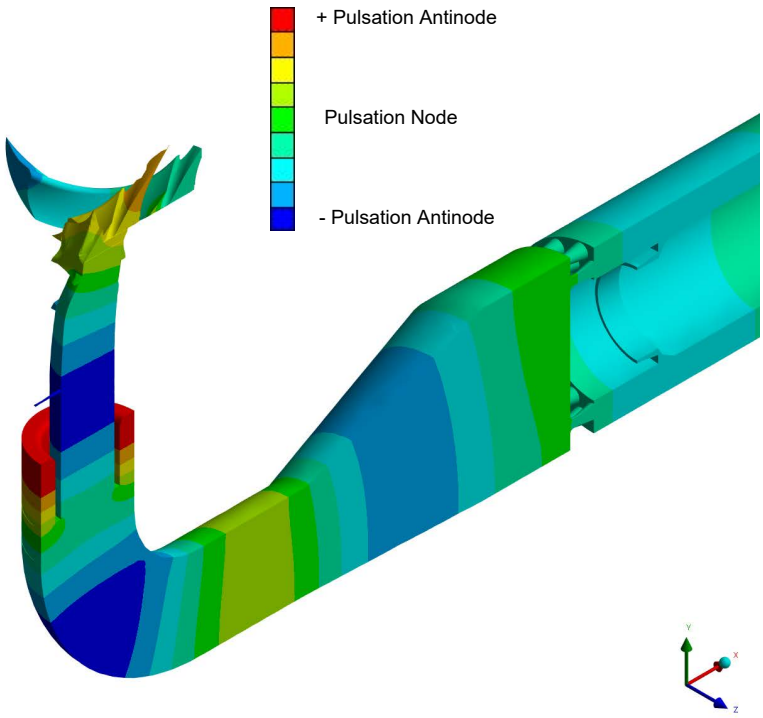

Figure 30: Acoustical mode shape at 524 Hz

Engineering Dynamics Incorporated
16117 University Oak, San Antonio, TX 78249
210-492-9100 www.engdyn.com

Design and 3-D Printing of Insert

To realize the geometry specified by the acoustical analyses, an "insert" for the compressor discharge cavity was conceived as shown in Figure 31. A 3-D scanner was used to determine the existing volume and shape of the compressor discharge cavity. The desired compressor internal geometry was then subtracted from that scan, resulting in the insert shown in Figure 31. The various holes that are shown were used to provide test ports for the insertion probes, and to allow an escape path to the process for any liquids that might be captured between the insert and the compressor case.

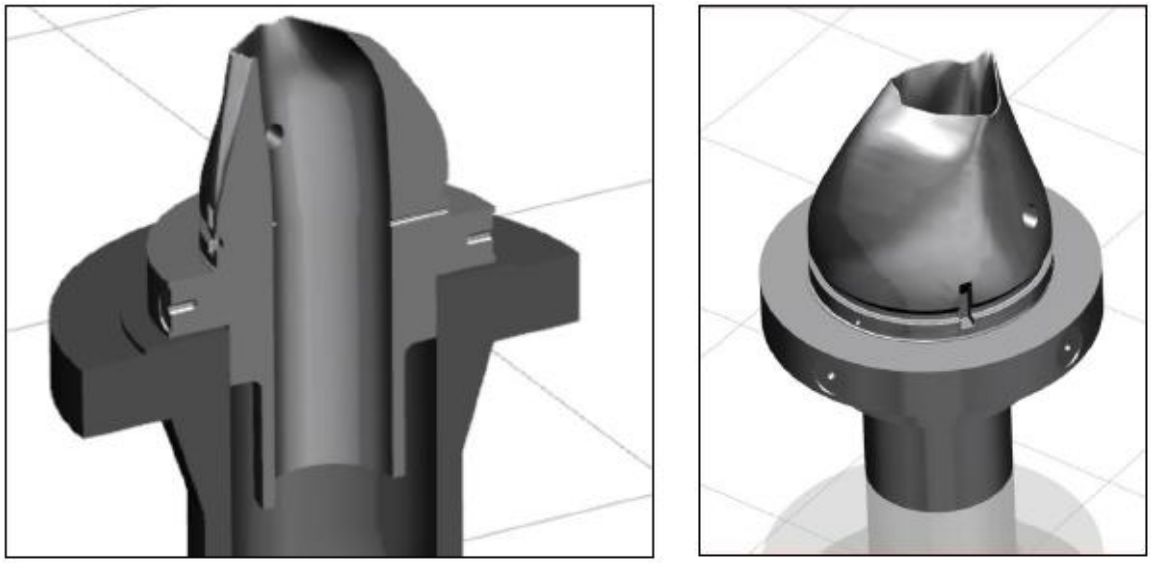

Figure 31: Discharge cavity insert

An additive manufacturing process (3-D printing) was available that could produce the desired insert. Initially, the part was produced in plastic to test-fit into the compressor case. After obtaining the final design, a different 3-D printer was used to produce the final part in Inconel, which is a high strength corrosion resistant nickel chromium steel alloy. The part was printed in a few days and installed into the compressor.

Test Stand Data

After the insert was fabricated and installed, the instrumentation and data acquisition was re-installed and the range of testing was repeated. The measured axial vibration amplitudes at 4× running speed with (green) and without (red) the insert are shown in Figure 32.

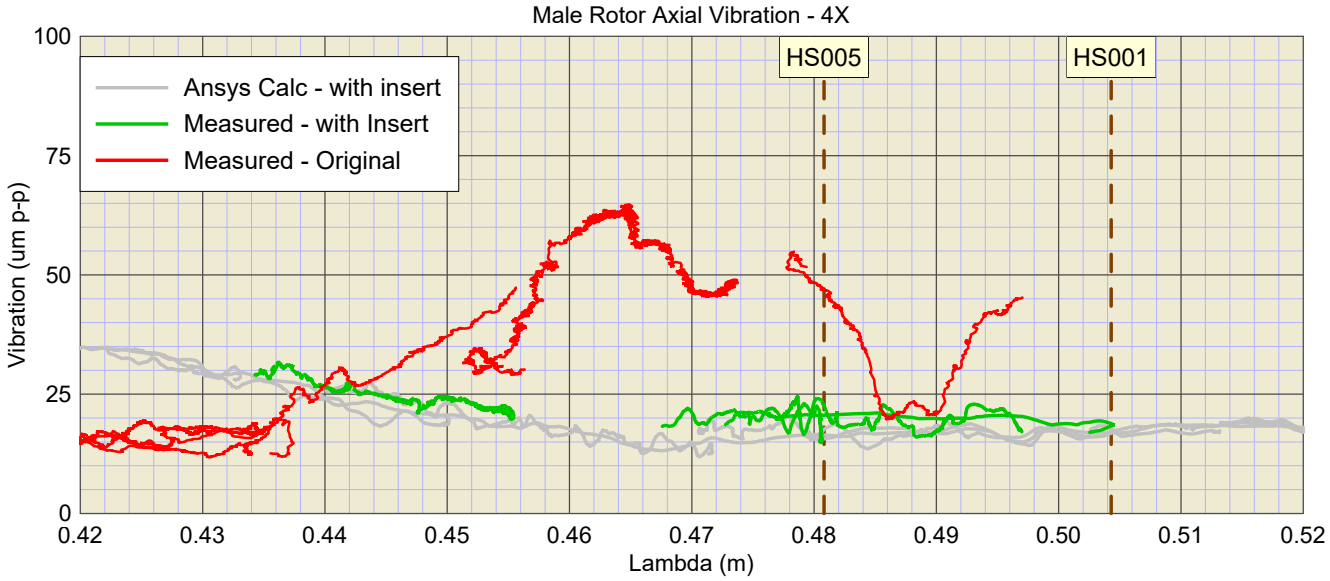

Figure 32: Comparison of axial vibration with and without insert

On the test stand, vibration amplitudes were reduced from 62 microns peak-peak to 23 microns peak-peak. For comparison to FEA results, the grey trace depicts unscaled pulsation at the rotor face calculated by the FEA model with the insert installed.

Field Data - Installation Testing

The compressor with the rotordynamic and acoustical cavity modifications was re-installed at the site. Vibration and pulsation instruments were connected as had been done for all previous field tests.

Phase one testing was intended to operate the compressor over the complete range of operating conditions, and included;

Phase 1A Normal operation with full forward flow

Phase 1B Maximum molecular weight gas

Phase 1C Off-design – minimum molecular weight gas.

Trend data for the axial vibration probes are shown in Figure 33. Vibration remained low (25–30 microns peak-peak, overall) for all gas compositions experienced. Other vibration test points showed similar low amplitude vibration.

Phase two conditions were for endurance testing. Data were monitored continuously as plant rates were increased to maximum. Monitoring continued for 8 days of typical operation, during which no adverse vibration occurred.

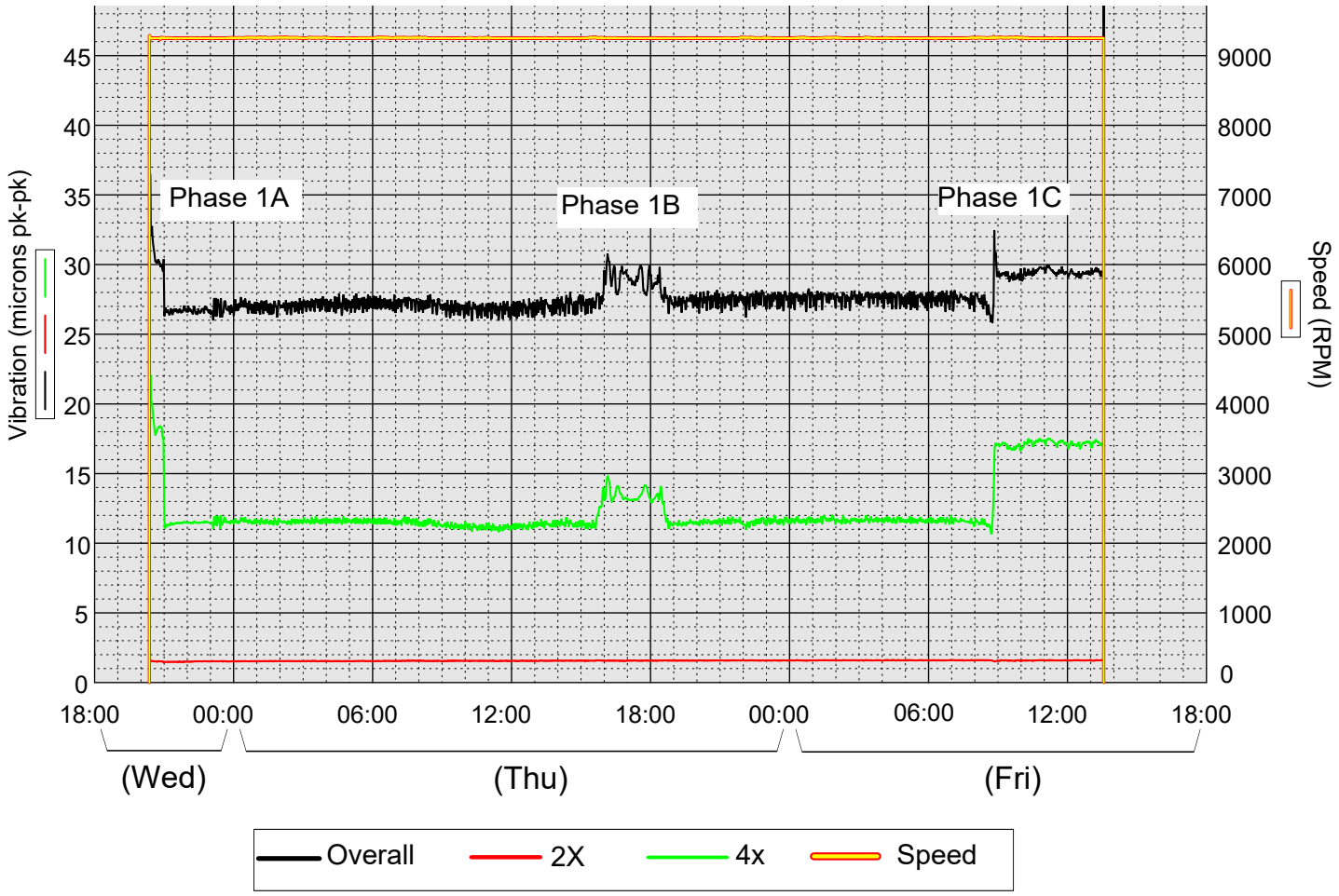

Figure 33: Modified compressor installed – stage 3 male rotor axial vibration

Engineering Dynamics Incorporated
16117 University Oak, San Antonio, TX 78249
210-492-9100 www.engdyn.com

CONCLUSIONS

Two resonance conditions, one acoustic-related and one rotordynamic, neither of which are typically considered in the design phase, combined to cause the damaging 2× axial vibrations. Several gas natural frequencies could become resonant with PPF excitation (4× running speed) due to molecular weight or suction temperature changes. When operating in such an acoustic resonance condition, the resulting high gas pulsation forces on the rotor caused axial vibrations to reach a large percentage of the thrust bearing's axial clearance. Occurring within a fluid film bearing, such large vibrations meant highly nonlinear forces were created by the bearing's oil film. These nonlinearities, together with an axial rotor mode in close proximity to half the 4× excitation, created the necessary conditions for a subharmonic resonance to occur with high 2× vibrations.

Encountering an axial subharmonic resonance in the field was one of several unique aspects of this problem and its resolution. Another was that the problematic acoustic mode was highly 3D in shape and very localized within the compressor's discharge cavity, making identification and modification difficult. As such, the typical approaches to alter or attenuate a GNF were ineffective and an unconventional approach was necessary, *i.e.*, modifying the discharge cavity itself using a 3D insert.

This experience resulted in a variety of lessons learned. For example, the GNFs in the discharge cavity that were predicted using the ANSYS® Fluid-30 element and verified with measured test data were very sensitive to volume at the compressor discharge, including into the exposed flutes. The analyst must specify the internal geometry carefully. Pulsation data in this region should be acquired with insertion probes, ideally placed near the antinodes of the suspected GNF. At the wavelengths experienced, a 150 mm change of position was required to obtain useful pulsation data.

On the test stand, it is often not possible to test machine response to the full range of expected speed of sound conditions. However, a variety of speed of sound conditions can be simulated (even though the test gas has constant properties) by varying machine speed, calculating λ, and plotting scaled pulsation amplitude versus λ rather than frequency. Although somewhat contrary to usual practices, this technique allows a more complete understanding of machinery cavity acoustics than could otherwise be obtained.

Since almost every machine is tested at the OEM before delivery to the customer, a wide database can be generated from future test runs or existing records to derive maps (scaled pulsation amplitude vs. lambda) with predictive operation behavior for geometrically similar compressors and downstream peripherals. This empirical approach could be considered at the design phase of future orders at a certain confidence level of available data. A comparison of different wave lengths from operating points on the job could be compared to the map and indicate whether design modifications or a 3D insert should be taken into account at least as a fall-back option.

It is possible to predict the problematic acoustical phenomena experienced using CFD methods. Both 360 degree and transient simulations can be used to generate a detailed representation of the time-domain flow conditions and pressure fields in the screw compressor. However, such calculations are so computationally expensive that it would not be practical to calculate large numbers of operating points. Instead, detailed information for specific cases can be generated to understand the origin of the acoustic excitation. Using that knowledge, the design can be optimized to reduce acoustical excitation. Additionally, geometric modifications such as damper elements can be specifically developed, and their effectiveness predicted. Using these techniques, simplified models for future machines can be developed and verified.

This paper describes an extraordinary story and learning curve. By far, not all mechanisms and chain of cause and effect are understood at the moment. However, it does describe the basic approaches for future R&D activities and provides a contribution to the general understanding and physics of the coexisting mechanical and acoustical resonance conditions in a dry screw compressor.

NOMENCLATURE

1A	=	First axial mode	
2A	=	Second axial mode	
API	=	American Petroleum Institute	
c	=	Speed of sound	
FEA	=	Finite element analysis	
FR	=	Compressor female rotor	
$F_{4\times}$	=	PPF force excitation	N 0-p
F_{act}	=	Film force from active thrust bearing	N
F_{inact}	=	Film force from active thrust bearing	N
F_{static}	=	Compressor static thrust load	N
GNF	=	Gas volume natural frequency	
K_{act}	=	Active thrust bearing oil film stiffness	
K_{HSG}	=	Bearing housing axial stiffness	
K_{RING}	=	Thrust ring axial stiffness	
L	=	Characteristic length	
MR	=	Compressor male rotor	
MW	=	Molecular weight	
PPF	=	Pocket passing frequency	
SHR	=	Subharmonic resonance	
TEF	=	Thrust bearing assembly total end float	
$z, \dot{z}, \ddot{z}$	=	Axial displacement, velocity and acceleration	
ζ	=	Damping ratio	%
λ	=	Acoustic wavelength	m
ω_d	=	Damped natural frequency	cpm

REFERENCES

[1] M. L. Adams, "Nonlinear dynamics of flexible multi-bearing rotors," *Journal of Sound and Vibration*, vol. 71, no. 1, pp. 129–144, 1980.

[2] API, *Axial and Centrifugal Compressors and Expander-compressors*, 9th ed. American Petroleum Institute, 2022, no. STD 617.

[3] J. H. Argyris and H. P. Mlenjnek, *Dynamics of Structures*. Elsevier Science, 1991.

[4] S. Berger, O. Bonneau, and J. Frêne, "Influence of axial thrust bearing on the dynamic behavior of an elastic shaft: Coupling between the axial dynamic behavior and the bending vibrations of a flexible shaft," *Journal of Vibration and Acoustics*, vol. 123, no. 2, pp. 145–149, 11 2000. [Online]. Available: https://doi.org/10.1115/1.1355243

[5] J. Burgess, *Harmonic, Superharmonic, and Subharmonic Response for Single Degree of Freedom Systems of the Duffing Type*. Stanford University, 1954. [Online]. Available: https://books.google.com/books?id=2JkUAAAAIAAJ

[6] J. M. Byrne, P. Potter, and J. A. Vázquez, "Gas seal failures caused by axial vibrations," in *Proceedings of the 47th Turbomachinery Symposium*. Texas A&M University. Turbomachinery Laboratories, 2018. [Online]. Available: https://hdl.handle.net/1969.1/175068

[7] I. Chatzisavvas, A. Boyaci, P. Koutsovasilis, and B. Schweizer, "Influence of hydrodynamic thrust bearings on the nonlinear oscillations of high-speed rotors," *Journal of Sound and Vibration*, vol. 380, pp. 224–241, 2016. [Online]. Available: https://www.sciencedirect.com/science/article/pii/S0022460X16301626

[8] D. W. Childs, "Fractional-frequency rotor motion due to nonsymmetric clearance effects," *ASME Journal of Engineering for Power*, vol. 104, pp. 533–541, July 1982.

[9] S. DeCamillo, "Axial subsynchronous vibration," in *Proceedings of the 43rd Turbomachinery Symposium*. Texas A&M University. Turbomachinery Laboratories, 2014. [Online]. Available: https://doi.org/10.21423/R1K35G

[10] G. Diana, F. Cheli, A. Collina, and S. Bruni, "Axial vibrations induced by oil film forces," in *Sixth International Conference on Vibrations in Rotating Machinery*. IMechE, September 1996, pp. 151–160.

[11] H. Dresig and F. HolzweiSSig, *Maschinendynamik*. Springer Verlag, 2013.

[12] G. Duffing, *Erzwungene Schwingungen bei veränderlicher Eigenfrequenz und ihre technische Bedeutung*. Vieweg & Sohn, 1918.

[13] D. Dyer, "Sub-rotational speed axial vibrations of shafts in rotating machinery," in *Third International Conference on Vibrations in Rotating Machinery*. IMechE, September 1984, pp. 439–446.

[14] F. F. Ehrich, "Subharmonic vibrations of rotors in bearing clearance," in *Design Engineering Conference and Show*, no. 66-MD-1. Chicago: ASME, May 1966.

[15] ——, "High order subharmonic response of high speed rotors in bearing clearance," *ASME Journal of Vibration, Acoustics, Stress and Reliability in Design*, vol. 110, pp. 9–16, January 1988.

[16] F. F. Ehrich, Ed., *Handbook of Rotordynamics*, 2nd ed. Krieger Publishing Company, 1999.

[17] R. Eisenmann and L. Santos-Gutierrez, "Dry gas seal failure due to axial sub-synchronous vibration on a hydrogen recycle gas compressor," in *Proceedings of the 47th Turbomachinery Symposium*. Texas A&M University. Turbomachinery Laboratories, 2018. [Online]. Available: https://hdl.handle.net/1969.1/175076

[18] M. He and J. M. Byrne, "Fundamentals of fluid film thrust bearing operation and modeling," in *Proceedings of the 51st Turbomachinery Symposium*. Texas A&M University. Turbomachinery Laboratories, 2022.

[19] D. Kiuchi, "Coupled sub-synchronous vibration of lateral and axial directions," in *Proceedings of the 40th Turbomachinery Symposium*. Texas A&M University. Turbomachinery Laboratories, 2011. [Online]. Available: https://doi.org/10.21423/R1JP85

[20] I. Kovacic and M. J. Brennan, *The Duffing Equation: Nonlinear Oscillators and their Behaviour*. John Wiley & Sons, 2011.

[21] C. Kraft and H. Schwarze, "Benutzeranleitung für das axialgleitlagerberechnungsprogramm COMBROS-A, version 1.4," TU Clausthal, Clausthal-Zellerfeld, Germany, Tech. Rep., 2017.

[22] R. S. Lord Rayleigh, "Xvii. on the maintenance of vibrations by forces of double frequency, and on the propagation of waves through a medium endowed with a periodic structure," *Philosophical Magazine Series 1*, vol. 24, pp. 145–159, 1887.

[23] K. Magnus, K. Popp, and W. Sextro, *Schwingungen: Physikalische Grundlagen und mathematische Behandlung von Schwingungen*. Springer Verlag, 2013.

[24] R. Marques and L. Ishimoto, "Radial subsynchronous vibration caused by axial vibration," in *Proceedings of the 48th Turbomachinery Symposium*. Texas A&M University. Turbomachinery Laboratories, 2019. [Online]. Available: https://hdl.handle.net/1969.1/188613

[25] E. Mujic, A. Kovacevic, N. Stosic, and I. Smith, *Advances in Noise Analysis, Mitigation and Control*, N. Ahmed, Ed. IntechOpen, 2016. [Online]. Available: https://doi.org/10.5772/61648

[26] T. F. Peixoto and K. L. Cavalca, "Thrust bearing coupling effects on the lateral dynamics of turbochargers," *Tribology International*, vol. 145, p. 106166, 2020. [Online]. Available: https://www.sciencedirect.com/science/article/pii/S0301679X20300104

[27] S. M. Price and D. R. Smith, "Sources and remedies of high-frequency piping vibration and noise," in *Proceedings of the 28th Turbomachinery Symposium*. Texas A&M University. Turbomachinery Laboratories, 1999. [Online]. Available: https://doi.org/10.21423/R1Z37N

[28] T. N. Shiau and W. C. Hsu, "A nonlinear analysis of the axial steady state response of the hydrodynamic thrust bearing-rotor system subjected to a harmonic excitation," in *ASME Turbo Expo 2005*, no. GT2005-68692. Reno-Tahoe, Nevada: ASME, June 2005, pp. 1–9.

[29] D. R. Smith, "Pulsation, vibration, and noise issues with wet and dry screw compressors," in *Proceedings of the Fortieth Turbomachinery Symposium*. Texas A&M University. Turbomachinery Laboratories, 2011. [Online]. Available: https://doi.org/10.21423/R1D64K

[30] N. Stošić, E. Mujić, A. Kovačević, and I. Smith, "Development of a rotor profile for silent screw compressor operation," in *International Conference Compressors and their Systems*, December 2007, pp. 133–145.

[31] A. Tondl, "Notes on the identification of subharmonic resonances of rotors," *Journal of Sound & Vibration*, vol. 31, no. 1, pp. 119,IN1–127,IN1, Nov. 1973.

[32] T. von Kármán, "The engineer grapples with nonlinear problems," *Bulletin of the American Mathematical Society*, vol. 46, no. 8, pp. 615 – 683, 1940. [Online]. Available: https://doi.org/

[33] B. C. Wen, W. Y. Wu, and D. J. Liu, "Dynamic characteristics of the rotors with axial vibration," in *International Conference on Rotordynamics*. Toyko, Japan: IFToMM, September 1986, pp. 577–582.

[34] J. J. Yu, "Axial vibration due to thrust bearing and its elimination," in *7th International Conference on Rotor Dynamics*. Vienna, Austria: IFToMM, September 2006.

[35] L. Zhao, "Axial vibration for a synchronous motor driven gear and in-line compressor train," in *Proceedings of the 42nd Turbomachinery Symposium*. Texas A&M University. Turbomachinery Laboratories, 2013. [Online]. Available: https://doi.org/10.21423/R1DH05

[36] Q. Zhu and W. J. Zhang, "A preliminary nonlinear analysis of the axial transient response of the sector-shaped hydrodynamic thrust bearing-rotor system," *ASME Journal of Tribology*, vol. 125, pp. 854–858, 2003.

ACKNOWLEDGEMENTS

The diagnosis and resolution of these challenging issues would not have been possible without valuable contributions from the authors' colleagues at ExxonMobil (Jonathan Toner, Yupiter Kristiyanto, Michael McCarter, Frank Kerze, Alex Kaverzin, Rotimi Ojifinni, Noel Hart, Eddie Del Pino), at SBM (Adam Bernays, Ayold Keulen, Shaun Brett, Erik Enzerink, Nicolas Bigle, Ronnes Ribeiro), at MAN Energy Solutions (Volker Browarzik, Markus Bothe, Udo Storcks, Alexander Heinz, Ralf Gödde, Norbert Tewes, Bernhard Barbosa, Thomas Müller, Dino Reichelt, Heinrich Bär, Irina Berg-Skandera, Roland Emmrich, Seyfi Türkmen, Kevin Schön, Sven-Hendrik Wiers, Jochen Domas), at EDI (Charles Hill, David Hanes, Brandon Laumer, Ken Atkins), and at BRG (José Vázquez, Minhui He, John Kocur, Keith Parsell, Eric Maslen).